Published in final edited form as:
Nat Cancer. 2020 December ; 1(12): 1153–1166. doi:10.1038/s43018-020-00133-0.

CD25-T_{reg}-depleting antibodies preserving IL-2 signaling on effector T cells enhance effector activation and antitumor immunity

Isabelle Solomon[1], **Maria Amann**[2], **Anne Goubier**[3], **Frederick Arce Vargas**[1], **Dimitrios Zervas**[1], **Chen Qing**[1], **Jake Y. Henry**[1], **Ehsan Ghorani**[1], **Ayse U Akarca**[6], **Teresa Marafioti**[6], **Anna Śledzińska**[1], **Mariana Werner Sunderland**[1], **Dafne Franz Demane**[1], **Joanne Ruth Clancy**[1], **Andrew Georgiou**[1], **Josephine Salimu**[3], **Pascal Merchiers**[3], **Mark Adrian Brown**[3], **Reto Flury**[2], **Jan Eckmann**[4], **Claudio Murgia**[2], **Johannes Sam**[2], **Bjoern Jacobsen**[5], **Estelle Marrer-Berger**[5], **Christophe Boetsch**[5], **Sara Belli**[5], **Lea Leibrock**[5], **Joerg Benz**[5], **Hans Koll**[4], **Roger Sutmuller**[2], **Karl S. Peggs**[1], **Sergio A. Quezada**[1]

[1]Cancer Immunology Unit, Research Department of Haematology, University College London Cancer Institute, London WC1E 6DD, UK [2]Roche Innovation Center Zurich, Roche Pharmaceutical Research and Early Development (pRED), Wagistrasse 10, 8952 Schlieren, Switzerland [3]Tusk Therapeutics Ltd, Stevenage Bioscience Catalyst, Gunnels Wood Road, Stevenage, Hertfordshire SG1 2FX, UK [4]Roche Innovation Center Munich, Roche Pharmaceutical Research and Development (pRED), Nonnenwald 2, 82377 Penzberg, Germany [5]Roche Innovation Center Basel, Roche Pharmaceutical Research and Development (pRED), Grenzacherstrasse 124, 4070 Basel, Switzerland [6]Department of Cellular Pathology, University College London Hospital, London NW1 2BU, UK

Abstract

Intratumoral regulatory T cell (Treg) abundance associates with diminished anti-tumor immunity and poor prognosis in human cancers. Recent work demonstrates that CD25, the high affinity receptor subunit for IL-2, is a selective target for Treg depletion in mouse and human

Correspondence to: Maria Amann; Karl S. Peggs; Sergio A. Quezada.

Correspondence: Maria Amann (Maria.Amann@Roche.com), Karl S. Peggs (k.peggs@ucl.ac.uk) and Sergio A. Quezada (s.quezada@ucl.ac.uk).

Author Contributions

S.A.Q. and K.S.P. conceived the project. I.S., M.A., E. M-B., B.J., J.B., A.G., K.S.P., and S.A.Q. designed the experiments, analyzed the data, and wrote the manuscript. I.S., A.G., J.S., P.M., M.A.B., J.S., R.F., L.L. and C.M. performed the experiments. D.Z., C.Q., J.E., M.W.S., D.F.D. and J.R.C. contributed experimentally. J.Y.H., C.B. S.B. contributed with analysis of the data. R.S., H.K., F.A.V. and A.S. contributed intellectually. Andrew Georgiou provided technical support

Competing Interests

A patent application WO/2018/167104, with relevance to this work has been filed by Cancer Research Technology Limited and Tusk Therapeutics and we want to declare our relationship with this patent. I.S. F.A.V., S.A.Q., K.S.P., A.G., J.S., P.M., are named inventors on these patents. F.A.V., S.A.Q., I.S. and K.S.P. receive royalties related to these patents. S.A.Q. is an advisor to TUSK/Roche. M.A., R.F., J.E., C.M., J.S., B.J., L.L., H.K., J.B., S.B., C.B., E. M-B. and R.S. are employees of Roche, which plan clinical development of the drug.
M.A., R.F., J.E., C.M., J.S., B.J., H.K., J.B., S.B., C.B., E. M-B. and R.S. have shares in the companies to which the patents belong.

Europe PMC Funders Author Manuscripts

malignancies; however, anti-human CD25 antibodies have failed to deliver clinical responses against solid tumors due to bystander IL-2 receptor signaling blockade on effector T cells, which limits their anti-tumor activity.

Here we demonstrate potent single-agent activity of anti-CD25 antibodies optimized to deplete Tregs whilst preserving IL-2-STAT5 signaling on effector T cells, and demonstrate synergy with immune checkpoint blockade in vivo. Pre-clinical evaluation of an anti-human CD25 (RG6292) antibody with equivalent features demonstrates, in both non-human primates and humanized mouse models, efficient Treg depletion with no overt immune-related toxicities. Our data supports the clinical development of RG6292 and evaluation of novel combination therapies incorporating non-IL-2 blocking anti-CD25 antibodies in clinical studies.

Introduction

Regulatory T cells (Treg) have key roles in the control of immune homeostasis, autoimmunity and anti-tumor immunity[1]. Several studies have linked Treg infiltration with poor prognosis in cancer[2–5]. Furthermore, the intratumoral balance between effector T cells (Teff) and Treg impacts on tumor progression and response to therapy[6,7]. Whilst these studies underscore the potential value of Treg as targets in cancer immunotherapy, there has been limited clinical success targeting this subset. There is no consensus on the most selective targets for Treg depletion, and limited mechanistic insight into the activity of Treg specific depleting antibodies in vivo. In mice, anti-CTLA-4 antibodies have been shown to preferentially deplete tumor infiltrating Treg via engagement with activating Fc receptors (FcRs)[8–10]. In humans, the Treg depleting activity of anti-CTLA-4 antibodies remains controversial, with some studies failing to show Treg reduction in patients[11] whilst others suggest that enhancing the affinity of anti-human CTLA-4 to FcRs could potentially improve clinical outcomes[12–14].

The interleukin-2 receptor alpha subunit (IL-2Rα, CD25) is a potential target based on higher expression on Treg versus Teff[15–17] cells. Lack of therapeutic activity of anti-CD25 monoclonal antibodies (mAbs) in mice and humans has, however, tempered enthusiasm for further development. We demonstrated that the lack of therapeutic activity of the most common anti-CD25 mAb (clone PC61) in mouse models of cancer was associated with poor binding to activating FcRs required for antibody dependent cell cytotoxicity/phagocytosis (ADCC/P). In contrast, an Fc-optimized anti-CD25 boosted the activity of anti-PD1 promoting complete responses[17]. It is notable that both anti-CD25 antibodies tested in the clinic, Daclizumab and Basiliximab[18,19], had been originally developed to prevent acute organ rejection and/or to treat multiple sclerosis through the blockade of IL-2 signaling required by autoreactive T cells. IL-2 blockade is also a feature of the anti-mouse CD25 mAb (Clone PC61) currently used to deplete Treg in mouse models of cancer[20].

Considering the critical role that IL-2 plays in Teff survival and function[21–23], we hypothesized that the in vivo activity of the available Treg depleting anti-CD25 mAbs were likely limited by their IL-2 blocking activity on the effector compartment. An anti-CD25 depleting mAb which does not interfere with IL-2 signaling should induce stronger effector responses and anti-tumor activity, even more so considering that Treg depletion will increase

Europe PMC Funders Author Manuscripts

locally available IL-2[24] to support Teff function. If correct, this insight offers a unique opportunity to develop highly specific and potent Treg depleting agents that target regulatory T cells via CD25 whilst preserving IL-2 signaling on Teffs.

Results

Characterization of non-IL-2 blocking anti-mouse CD25 mAbs (αCD25^{NIB})

We previously demonstrated that when the commonly used αCD25 clone PC61 was converted to a depleting mIgG2a isotype (αCD25^{PC61}), it synergized with anti-PD1 to reject established tumors[17]. However, αCD25^{PC61} also interferes with IL-2 signaling on Teff. Anti-CD25 clone 7D4 is a non-depleting IgM which binds to mouse CD25 without blocking IL-2 signaling[20,25]. By resolving the variable region of 7D4 and cloning it into a mouse IgG2a backbone, we generated a depleting, non IL-2 blocking antibody (αCD25^{NIB}) for comparison.

The IL-2 blocking activity of αCD25^{NIB} and αCD25^{PC61} was compared by quantification of phosphorylated STAT5 (pSTAT5), downstream of IL-2R signaling. CD3^{+} T cells from C57BL6 splenocytes were stimulated with 50U/ml of IL-2 in the presence of αCD25 antibodies or a control αIL-2 neutralizing antibody (nAb). No pSTAT5 signaling was observed in CD8^{+} or CD4^{+} Teff, which express low to undetectable levels of surface CD25 in naïve animals. IL-2 stimulation increased pSTAT5 expression by approximately 50% on CD25^{high} Tregs. Pre-treatment of the cells with αCD25^{NIB} did not affect pSTAT5 levels. In contrast, αCD25^{PC61} induced a 50% reduction in pSTAT5 whilst IL-2 neutralization ablated the pSTAT5 signal (Fig. 1a and b). Considering the fact that the αCD25^{NIB} did not interfere with pSTAT-5 (which sits upstream of the IL-2 signaling cascade), we did not pursue further evaluation of the potential impact of αCD25^{NIB} in downstream components of IL2R signalling.

We next evaluated whether these mAbs would interfere with IL-2 signaling in antigen experienced tumor infiltrating lymphocytes (TILs). Mice were challenged with MCA205 tumor cells, and at days 5, 10 and 14 left untreated or treated with αCD25^{PC61} or αCD25^{NIB}. One day after the last dose of mAb, mice were sacrificed and TILs isolated for pSTAT5 analysis ex-vivo, post re-exposure to IL-2 (Fig. 1c). In Teff, pSTAT5 signaling was significantly reduced by αCD25^{PC61} whereas αCD25^{NIB} had no impact compared to untreated TILs. In Treg, both αCD25^{PC61} and αCD25^{NIB} reduced pSTAT5 signaling, although to a much lesser extent with αCD25^{NIB} (Fig. 1d). Considering that the amount of bound αCD25 could be reduced during tissue processing, we re-incubated TIL samples with the same antibodies administered in vivo. When TILs were re-exposed to αCD25^{PC61} or αCD25^{NIB} post isolation, αCD25^{PC61} completely abolished pSTAT5 signaling in CD8^{+} and CD4^{+} Teff cells as well as in the few remaining Treg cells relative to the untreated control (Fig. 1e and f). In contrast, no significant reduction in pSTAT5 was observed when comparing CD8^{+} and CD4^{+} Teff cells from αCD25^{NIB} treated TILS versus untreated. A small, albeit significant decrease in pSTAT5 was observed in Treg cells treated with αCD25^{NIB}. Of relevance, only a very small number of events were analyzed in this treatment group as the αCD25^{NIB} promoted depletion of tumor infiltrating Treg cells (Fig.

1f)._These data confirm that, in contrast to αCD25^{PC61}, αCD25^{NIB} does not block Teff IL-2 signaling in vitro or ex-vivo.

αCD25^{NIB} promotes rejection of established tumors

We next sought to compare the activity of αCD25^{NIB} and αCD25^{PC61} in vivo in different syngeneic tumor models. A single dose of αCD25^{NIB} promoted complete tumor rejection and long-term survival, with 10/10 and 8/10 mice remaining free of CT26 or MC38 tumors up to 70 days, respectively. In contrast, only 1/10 or 6/10 mice rejected CT26 or MC38 tumors when treated with a single dose of the IL-2-blocking αCD25^{PC61} (Fig. 2a and 2b).

As CD25 is upregulated on cells exposed to IL-2 in vitro[26], we sought to exclude the possibility of CD25^{+} effector T cell depletion by treating mice with multiple weekly doses of αCD25^{NIB}. Mice were challenged with MCA205 tumors and received either one dose or five doses (weekly) of the αCD25^{NIB} antibody. Both groups achieved significant tumor control with 9/15 and 14/15 complete responses. Multiple doses of the αCD25^{NIB} significantly increased complete responses compared to a single dose, arguing against a significant detrimental depletion of effector T cell populations critical for anti-tumor activity (Fig. 2c).

To determine whether the difference in the therapeutic activity of αCD25^{PC61} and αCD25^{NIB} was due to their relative IL-2 blocking capabilities, we treated MCA205-bearing mice with αCD25^{NIB} and neutralized IL-2 signaling with either an anti-IL-2 neutralizing mAb or the IL-2-blocking αCD25^{PC61} (Fig. 2d). Both ablated the therapeutic activity of αCD25^{NIB} confirming the critical role of IL-2 in tumor control, and suggesting that lack of single agent activity of αCD25^{PC61} (and potentially Daclizumab and Basiliximab) could relate to their IL-2 blocking activity (Fig. 2d). Similar results were observed in the CT26 colorectal carcinoma model, with tumor control only achieved in mice treated with αCD25^{NIB}, and loss of control observed upon IL-2 neutralization or αCD25^{PC61} treatment (Extended Data Fig. 1).

αCD25^{NIB} and αCD25^{PC61} promote equivalent Treg depletion but different Teff activation in vivo

Mice were challenged with MCA205 tumors, treated on day 5 and sacrificed at day 12 for analysis. Both αCD25^{PC61} and αCD25^{NIB} induced similar levels of intra-tumoral Treg depletion measured as percentage and absolute number of FoxP3^{+} T cells (Fig. 3a, 3b and 3c). Interestingly, whilst both antibodies significantly increased the CD8^{+}/Treg, CD4^{+}eff/Treg and NK/Treg cell ratios, αCD25^{PC61} had a bigger (although not statistically significant) impact on the ratio of effector to regulatory T cells within tumors (Fig. 3d), potentially due to the slightly higher reduction in Treg frequency induced by αCD25^{PC61} (Fig. 3b). Despite this apparent difference, αCD25^{NIB} induced the highest levels of T cell activation (~80% of CD8^{+} TILs Granzyme B^{+} compared to 50% in αCD25^{PC61} treated and 65% in untreated mice), with a similar trend in the CD4^{+} Teff and NK compartment. Importantly, αCD25^{PC61} lowered the levels of Granzyme B expression by tumor infiltrating CD8^{+} T cells. Lastly, IL-2 neutralization ablated the positive impact of αCD25^{NIB} on Granzyme B expression in TILs (Fig 3e, f, g). Levels of Granzyme B expression by CD8^{+}

and CD4^{+} T cells were equivalent in mice treated with αCD25^{PC61} and those treated with αCD25^{NIB} plus the neutralizing anti-IL-2 mAb (Fig 3e, g) underscoring the relevance of endogenous IL-2 and detrimental impact of IL-2 blockade on TIL function.

Similar patterns of Treg depletion and effector cells Granzyme B expression were observed in the MC38 model (Extended Data Fig. 2). These findings suggest that IL-2 availability post Treg depletion is critical to the superior anti-tumor activity of αCD25^{NIB}.

αCD25^{NIB} as a substrate for combination immunotherapy

We evaluated the ability of αCD25^{NIB} to synergize with αPD-L1. Mice challenged with MCA205 tumors and treated with αPD-L1 (clone 10F.9G2) on days 6, 9, 12 and 18 exhibit a short period of tumor control (between days 10 and 20) followed by tumor relapse (Fig. 4a). Combination with a single dose of αCD25^{NIB} at day 10 induced a 52% complete response rate ($p<0.0001$), whilst a second dose of αCD25^{NIB} on day 15 led to a 70% complete response rate (Fig. 4a).

We next evaluated the activity of αCD25^{NIB} against the poorly immunogenic B16BL6 mouse melanoma model[27]. Mice were challenged with B16BL6 tumors and left untreated or treated with Gvax (irradiated B16BL6 genetically modified to secrete granulocyte-macrophage colony-stimulating factor (GM-CSF)) to boost T cell infiltration[6,27], αCD25^{NIB} or a combination thereof. Gvax monotherapy did not affect tumor progression, whilst αCD25^{NIB} did delay tumor growth in a small percentage of animals. Combination therapy induced tumor regression in 90% of animals, delaying tumor progression and significantly increasing overall survival (Fig. 4b).

A parallel group of animals was sacrificed on day 15 for mechanistic studies by flow cytometry with a high dimensional panel designed to interrogate features of TIL activation. Unsupervised analysis of cytometry data characterized 20 TIL clusters across treatment groups (annotated in Fig. 4c). We identified resting and activated Treg populations (clusters 14 and 15 respectively) with differential expression of markers including CD25, PD1 and 41BB. Whilst anti-CD25^{NIB} monotherapy reduced the abundance of both Treg populations versus control, only the reduction of CD25^{hi} cluster 15 reached statistical significance. Whilst this cluster was expanded by Gvax monotherapy, combination treatment resulted in a significant depletion of both Treg clusters (Fig. 4d and e). Anti-CD25^{NIB} alone or in combination with Gvax resulted in a significant repatterning of the effector TIL landscape, with an increase in abundance of both CD4 (cluster 6) and CD8 (cluster 2) populations with features of high proliferation (Ki67^{hi}) but low activation status. Such populations have previously been associated with early differentiated memory responses important for sustaining tumour immune control[28,29]. In parallel, anti-CD25^{NIB} treatment resulted in a depletion of CD25^{hi} activated CD4 T cells (clusters 10-13), without loss of activated CD8 populations that had lower CD25 expression. Indeed, combined therapy significantly increased the abundance of activated CD8 clusters 3 and 5 (Fig. 4d and e), suggesting the greater clinical efficacy of the combination may be attributable to simultaneous depletion of Tregs and skewing of the effector compartment towards a greater abundance of both proliferating early differentiated T cells and activated CD8s._Taken together, these data

support future clinical evaluation of combination therapies incorporating depleting but non IL2-blocking αCD25 mAbs.

A novel anti-human CD25^{NIB} promotes effective Treg depletion in patient-derived tumor samples in vitro

Based on these findings, we next sought to develop a first-in-class anti-human CD25 antibody with similar characteristics. Forty-three anti-CD25 antibodies were generated (see methods) and selected on recombinant human and cynomolgus CD25. These were evaluated by flow cytometry for their ability to bind to human Treg, to not interfere with IL-2 signaling in a STAT5 phosphorylation assay, and to deplete human Treg in ADCC and ADCP assays (Extended Data Fig. 3). The best candidate was synthetized in an a-fucosylated format to deliver maximal depleting activity in vivo. This became our lead clinical candidate anti-human CD25^{NIB} and was named RG6292. RG6292 (FF) is the fully fucosylated version of RG6292. The IL-2-blocking activity of RG6292 (FF) was compared to that of Daclizumab through assessment of STAT5 phosphorylation. Both antibodies bound with similar affinity to human CD25^{+} cells (Extended Data Fig. 3a), but Daclizumab ablated STAT5 phosphorylation, whilst RG6292 (FF) did not significantly affect pSTAT5 in Treg, CD4+ or CD8+ T cells (Fig. 5a). Furthermore, Daclizumab and an IL-2 neutralizing antibody, but not RG6292 (FF), significantly decreased Granzyme B expression and proliferation of activated CD8^{+} and CD4^{+} T cells compared to the negative controls (Fig. 5b).

To characterize the binding of RG6292 to CD25, we crystalized a complex made from deglycosylated human CD25 and the Fab of RG6292. RG6292 bound to CD25 on the opposite side to the IL2-CD25 interaction site, consistent with lacking IL-2 signaling interference (Fig. 5c). The Treg depleting capacity of RG6292 and RG6292 (FF), was compared in co-cultures of purified, IL-2 activated NK cells or MCSF differentiated macrophages and in vitro differentiated Treg. RG6292 led to up to 80% specific lysis of Treg, compared to 60% lysis by RG6292 (FF) (Extended Data Fig. 3d). As for ADCP, both RG6292 and RG6292 (FF) promoted effective phagocytosis of Treg targets when compared to the hIgG1 isotype control (Extended Data Fig. 3e).

We next evaluated the combined ADCP and ADCC potential of RG6292 on activated CD8^{+} T cells versus Treg during polyclonal activation of human PBMC. CFSE labelled human PBMC were activated with anti-CD3 in vitro for 72 hours (see methods) in the presence of RG6292, or hIgG1 isotype control. For two independent donors, incubation with RG6292 led to 80% lysis of Treg compared to the hIgG1 isotype control (2 way Anova, Dunnet, $p < 0.001$), with a lesser impact (up to 25%) on activated CD4^{+} T cells, and no significant impact on activated CD8^{+} T cells (Fig. 5d). In both donors, preferential depletion of Treg over activated CD4^{+} and CD8^{+} T cells correlated with CD25 expression level in each subset (Fig. 5d and e).

Lastly, we evaluated the ability of RG6292 and RG6292 (FF) to deplete Treg in human tumor samples in vitro. Single cell suspensions from lung and colorectal cancer samples were supplemented with IL-2-activated NK cells and incubated with anti-CD25 or control antibodies for three hours. Both the RG6292 and RG6292 (FF) effectively depleted

$CD4^+FoxP3^+CD25^+$ cells within tumor samples, compared to controls (Fig. 5f and g). In contrast, $CD8^+$ cell numbers were not significantly affected between the different treatment groups (Fig. 5f and g), supporting effective and preferential targeting of $CD4^+FoxP3^+CD25^+$ cells within tumors. The data confirms that the anti-human CD25 antibody RG6292 does not block IL-2 signaling, is capable of eliciting ADCC and ADCP, and preferentially depletes Treg in vitro and in tumor samples from cancer patients.

Anti-human-$CD25^{NIB}$ (RG6292) depletes Treg and drives T cell activation in tumor-bearing humanized mice

To validate the Treg depleting activity of RG6292 in vivo, we used humanized tumor-bearing mice reconstituted with human immune T cell populations (see methods). Humanized mice were challenged with the human BxPC-3 pancreatic cancer cell line and treated 17 days later with vehicle, RG6292 (Fig. 6a and b) or anti-human CTLA-4 (Extended Data Fig. 4).

Cohorts were sacrificed and harvested (tumor, spleen and PBMCs) at days 1, 3, 4, 7 and 14 after treatment, and evaluated for Treg depletion and T cell activation by flow cytometry. Compared to the vehicle control, RG6292 decreased systemic and intra-tumoral Treg in a dose dependent manner (Fig. 6b upper panel), whilst increasing Granzyme B expression by $CD8^+$ T cells (Fig. 6a, b lower panel). At the highest dose of RG6292 (10mg/kg), Treg depletion in blood, spleen and tumor lasted for at least 14 days, whilst lower doses ≤ [1 mg/kg] were associated with recovery of Treg in blood and spleen, but not completely within tumors.

Whilst anti-CTLA-4 (Ipilimumab) also prompted Treg depletion in this model, RG6292 had the highest impact increasing the Teff/Treg ratio (Extended Data Fig. 4a). In blood and spleen, RG6292 showed similar ability to reduce Treg whereas Ipilimumab showed less consistent changes in Treg numbers (Fig. 6b and Extended Data Fig. 4a). Lastly, significant activation of tumor infiltrating $CD8^+$ T cells was only observed in mice treated with RG6292, as evidenced by an increase in the expression (MFI, %) of Granzyme B, HLA-DR, PD-1 and CTLA-4 (Fig. 6b lower panel and Extended Data Fig. 4b). We could also confirm a significant intratumoral increase of IL-2 on day 4 in the 10 and 1 mg/kg treated group (data not shown). CD25 expression was low on Treg after RG6292 and high after ipilimumab mediated depletion (Extended Data Fig. 4c).

Anti-human-$CD25^{NIB}$ (RG6292) depletes Treg in cynomolgus monkeys with no clear signs of autoimmune toxicities

The toxicity and pharmacokinetic/pharmacodynamic (PK/PD) profile of RG6292 was evaluated in cynomolgus monkeys following once every two weeks (Q2W, Fig. 6c) or weekly (Fig. 6d) intravenous administrations (0.1, 1, 10 mg/kg/dose) over 4 (Fig. 6d) and 2 weeks (Fig. 6c), respectively. Treg depletion was dose dependent, with maximal peripheral Treg depletion at doses ≥ 1 mg/kg sustained for at least 7 days (Fig. 6c). In the 4-week toxicity study, supra-pharmacological doses (10, 30 and 100 mg/kg/dose Q2W) were selected to investigate potential toxicities associated with Treg depletion within tissues. Despite systemic Treg depletion, the only drug-related toxicity finding was an exacerbation

of ulcerative/erosive rhinitis at 30 and 100 mg/kg, characterized by (partial) loss of epithelium accompanied by inflammatory cell infiltrates in the nasal cavities in individual animals (Fig. 6d). Of relevance, during the acclimatization phase, sneezing and nasal/muzzle discharges were reported in a few animals diagnosed with a viral upper respiratory tract infection. Only in animals treated with RG6292, we observed aggravated virus-triggered lesions, suggesting that pre-existing or concomitant local infection together with the RG6292-induced local Treg depletion led to an exacerbated inflammation. Noteworthy, there were no signs of active viral infection in the organs investigated and after a 4-week recovery period, reversibility of the nasal lesions was demonstrated. Together the data supports the Treg depleting capacity of RG6292 and its ability to exacerbate immunity without overwhelming signs of toxicity. Consistent with the lack of toxicity observed in cynomolgus monkeys, no signs of toxicity were observed in mice treated with multiple doses of $\alpha CD25^{NIB}$ (data not shown). An open label multicenter phase I study to evaluate safety, tolerability and PK/PD of RG6292 is currently open (NCT04158583).

Discussion

Treg depleting strategies have been extensively investigated as an approach to enhance anti-tumor immune responses, with the primary limitation being the identification of targets expressed differentially on Treg. Whilst several agents have been evaluated clinically, success remains limited. More recently, it has been shown that ADCC-enabled antibodies directed to immune modulatory receptors such as CTLA-4, OX40 and GITR, can also deplete Treg in mouse tumor models, supporting the development of “dual activity antibodies”. These would eliminate Treg expressing high levels of the target receptor whilst blocking a co-inhibitory signal (CTLA-4) or delivering an activating signal (OX-40, GITR) to Teff expressing lower levels of the same receptor[8,12,30–32]. Upregulation of CTLA-4, OX-40 or GITR on activated Teff[33] could also result in their partial depletion, especially in the context of the new generation of ADCC-enhanced antibodies[13,34] (i.e. a-fucosylated CTLA-4), highlighting the need for more specific targets.

We recently demonstrated that CD25 is expressed at high levels on Treg in mice and humans but at lower levels on $FoxP3^{-}CD4^{+}$ cells, and almost undetectable levels on tumor infiltrating $CD8^{+}$ T cells[17]. In humans this expression pattern is retained even in the context of anti-PD-1 therapy[17]. This selective expression pattern, however, has not been leveraged to deliver significant anti-tumor responses, with currently available anti-human CD25 mAbs having been designed to block IL-2 signaling rather than to deplete Treg[19,35].

Our data demonstrate the critical importance of endogenous IL-2 to the function of the $CD4^{+}$ and $CD8^{+}$ effector compartments in the context of Treg depletion. Despite the very low levels of surface CD25 expression by tumor infiltrating $CD8^{+}$ T cells[17], anti-$CD25^{PC61}$ ablated pSTAT5 in these cells. In addition to depleting Treg, blockade of IL-2 signaling on tumor infiltrating effector T cells by anti-$CD25^{PC61}$ resulted in reduced T cell cytotoxicity and tumor control. An ADCC-enabled anti-CD25 mAb lacking IL-2 blocking activity (anti-$CD25^{NIB}$) demonstrated superior T cell activation and tumor control as a single agent against established mouse tumors. Based on these data we developed a novel non-IL-2-blocking human anti-human $CD25^{NIB}$ (RG6292). This was generated in an enhanced ADCC

format to enable maximal depleting activity in the tumor where high levels of the inhibitory FcRIIB (CD32B) are usually found[17]. Although we did not formally assess whether macrophages or NK cells were the mediators of Treg depletion, the data from the human anti-CD25 in Fig. 5. shows the ability of the RG6292 mAb to interact with both CD16 and CD32a, suggesting that if present, both macrophages and NK cells should be able to drive Treg depletion. Of relevance, in mouse models of cancer, we have previously shown that Treg depletion by antibodies targeting CTLA-4 can proceed in an NK and complement independent manner and primarily via myeloid cells[36]. The final effector of Treg depletion in vivo in humans would likely differ between tumour types, depending on the presence of innate effector subsets._Consistent with the mouse data, RG6292 effectively depleted human Treg whilst preserving IL-2R signaling on Teff, whereas Daclizumab, reduced both IL-2R signaling and T cell activation. Evaluation of our clinical lead in humanized mouse models also showed reduction in Treg compared to control, coupled to increased $CD8^+$ T cell activation in tumors. In the same experimental model, anti-CTLA-4 (Ipilimumab) showed Treg depleting activity but failed to significantly increase $CD8^+$ T cell activation. The potent single agent activity of anti-$CD25^{NIB}$ in immunogenic mouse tumor models characterized by Treg infiltration, suggests potential targets for future evaluation of RG6292 i.e. human malignancies that are known to be immunogenic in which Treg infiltration appears to correlate adversely with clinical outcomes (melanoma, lung cancer, head and neck and Microsatellite Instability-Hi (MSI-H) tumors). Our data also support evaluation in combination studies, since late intervention with αCD25^{NIB} in MCA205 bearing mice undergoing anti-PD-L1 treatment prevented tumor relapse in almost 50% of the cases, and the agent synergizes well with an anti-tumor vaccine in a poorly immunogenic melanoma model. Clinical evaluation of concomitant versus sequential delivery of RG6292 with PD-1/PD-L1 blocking agents will be needed to optimize scheduling. The data thus far suggest that anti-$CD25^{NIB}$ can be administered repeatedly as a single-agent, or alternated with anti-PD-L1, yielding significantly better tumor control.

Manipulation of Treg numbers or function is potentially associated with toxicity. Sustained systemic depletion promotes severe toxicities in mouse models such as the FoxP3-DTR model[37]. Anti-$CD25^{NIB}$ fails to completely deplete Treg, with a maximum of 60% depletion in our models. This partial depletion may be important with respect to the lack of toxicity seen in mice repeatedly treated with ADCC-enabled anti-CD25 mAbs[17] or with the anti-$CD25^{NIB}$ used in this study (data not shown). In cynomolgus monkeys RG6292 showed limited toxicities only at the highest, supra-pharmacological doses. If toxicities are observed in clinical trials, future pre-clinical work with anti-$CD25^{NIB}$ antibodies may aim to target activity to the tumor site, either by local intra-tumor administration or by antibody engineering approaches such as bispecific mAbs targeting CD25 and a tumor target, or masked pro-antibody approaches with activation within the tumor microenvironment.

In conclusion, our data demonstrate that targeting CD25 with a single dose of ADCC-enabled mAb preserving IL-2 signaling is a novel and powerful strategy to promote rejection of established tumors, delivering both depletion of Treg and enhanced, cell-intrinsic IL-2-driven Teff activation. RG6292 is the first anti-human CD25 antibody developed to mirror these attributes and provides a novel therapeutic substrate for combination in cancer immunotherapy.

Materials and Methods

Mice

C57BL/6, BALB/c, C57BL/6-Foxp3tm1Flv/J and NOD.Cg-Prkdc^{scid}IL-2rg^{tm1Wjl}/SzJ (NSG) mice were obtained from Charles River Laboratories. All animal studies were performed under either University College of London/ Charles River and UK Home Office ethical approval and regulations, or under local Swiss government ethical approval and regulations (license ZH193/2014) according to international FELASA and national GV-Solas and TierSchG guidelines, respectively. After arrival, animals were maintained for one week to get accustomed to the new environment and for observation. Mice were maintained under specific-pathogen-free conditions with daily cycles of 12 h light /12 h darkness according to committed guidelines (GV-Solas; Felasa; TierschG). Continuous health monitoring was carried out on a regular basis. For humanization, mice were injected with Busulfan (15 mg/kg) followed 24 hours later by an injection of human CD34^{+} cord blood cells (1*10^{5} per mouse; STEMCELL Technologies) as described earlier[39]. 5 days before tumor cell inoculation, humanized mice were screened for human T-cell frequencies by flow cytometry and only mice with more than 20% huCD45^{+} cells were randomized into different treatment groups. Mainly human adaptive immune cells (B and T cells, including Tregs) develop in this model whereas human myeloid cells as well as NK cells are only found in very low numbers. The formation of human secondary lymphoid organs, e.g. lymph nodes, and therefore adaptive memory formation is limited in this model. Tregs act in a cell contact dependent and autocrine manner on adaptive as well as innate immune cells. The incomplete cross-reactivity between mouse and human immune cells in this hybrid model precludes using it as toxicity or efficacy model for RG6292, but allows the primary pharmacodynamics to be monitored.

Cell lines, antibodies and tissue culture

MCA205 tumor cells (a kind gift from G. Kroemer, Gustave Roussy Cancer Institute) were cultured in Dulbecco's modified Eagle medium (DMEM, Sigma) supplemented with 10% fetal calf serum (FCS, Sigma), 100 U/mL penicillin, 100 μg/mL streptomycin and 2 mM L-glutamine (all from Gibco). CT26, MC38 and B16BL6 tumor cells were cultured in Roswell Park Memorial Institute medium (RPMI, Sigma) supplemented with 10% fetal calf serum (FCS, Sigma), 100 U/mL penicillin, 100 μg/mL streptomycin and 2 mM L-glutamine (all from Gibco). BxPC3 (ECACC) were cultured in RPMI 1640 medium (Gibco) containing 10% FCS (Gibco) and 1 x Glutamax (Invitrogen/ Gibco). SU-DHL1 tumor cells (DMSZ) were cultured in RPMI 1640 medium (Gibco) containing 10% FCS (Gibco). HSC-F (JCRB) suspension cells were cultured in RPMI 1640 medium (Gibco) containing 10% FCS (Gibco) and 1 x Glutamax (Invitrogen/ Gibco) and Glucose (2 g/L).

Basiliximab (Absolute Antibody; CuNo.: Ab00188-10.0) and Daclizumab (Absolute Antibody; CuNo.: Ab00187-10.0) were produced as human IgG1 antibodies, without the implementation of any a-fucosylation strategy. Ipilimumab (YERVOY®, BMS) is a human IgG1 isotype. The antibodies against mouse CD25 (clone PC61 and clone 7D4) were produced at Evitria and Absolute Antibody as mIgG2a. Under identical assay conditions, (using BIAcore© B2000 instrument, (GE Healthcare)) both antibodies showed similar Kd

values (2.6 nM for 3.6 nM for… data not shown) indicating comparable binding strength to mouse CD25. The mouse IL-2 neutralizing antibody (JES6-1A12) and anti-PD-L1 antibody (10F.9G2) were purchased at BioXcell (BioXcell). Isotype controls were the mouse IgG2a isotype control (eBM2a, ThermoFisher) and the Ultra-LEAF™ purified human IgG1 isotype control (QA16A12, Biolegend).

RG6292[40] is an a-fucosylated human IgG1 mAb produced using GlymaxX technology[41] with enhanced ADCC capacity. RG6292 was also produced without implementation of any a-fucosylation strategies (RG6292 FF) and in an Fc silent format with abolished FcγR and C1q binding by introduction of P329G/Leu234Ala/Leu235Ala Fc-mutations[42].

In vivo tumor experiments

Cultured mouse tumor cells were trypsinized, washed and resuspended in PBS and injected intra dermally (i.d.) in the flank, with or without Matrigel, depending on the model (number of cells injected indicated in figure legends). BxPC3 tumor cells (1x 10^6 cells) were injected s.c. in female stem cell humanized NSG mice in 50% growth factor–reduced Matrigel admixed with 50% RPMI. Antibodies were injected intraperitoneally (i.p.) and intravenously (i.v.), respectively, at the time points described in the figure legends. For functional experiments, blood and tissues were harvested and processed at the time points indicated in the legends. Spleen, lymph nodes (inguinal, axillary, and brachial) and tumors were dissected into RPMI. Mouse tumors were mechanically disrupted using scissors, digested with a mixture of 0.33 mg/ml DNase (Sigma-Aldrich) and 0.27 mg/ml Liberase TL (Roche) in serum-free RPMI for 30 min. A single cell suspension of BxPC3 tumors was prepared by using the gentleMACS Dissociator (Miltenyi Biotec) followed by digestion for 30 minutes with 0.025 mg/ml DNAse I (RocheDiagnostics) and 1 mg/ml Collagenase D (RocheDiagnostics). Tumor digest, spleen and lymph nodes were dispersed through a 70-μm filter. Erythrolysis of whole blood and spleen samples were performed using the BD Pharm Lyse buffer (BD).

For tumor growth and control experiments, tumors were measured twice weekly and volumes calculated as the product of three orthogonal diameters. Mice were euthanized when any diameter reached 150mm.

PhosphoSTAT5 evaluation

Pan T cells were isolated from splenocytes using the Dynabeads FlowComp™ Mouse Pan T (CD90.2) kit. 200,000 mouse T cells and human PBMC, in complete RPMI were plated and rested for 2-3 hours at 37°C. Antibodies (mouse: αCD25^{PC61} or anti CD25^{NIB} (both mIgG2a), αIL-2 neutralizing antibody (nAb) (JES6-1A12, BioXcell); human: RG6292, human IgG1 isotype control, Basiliximab (Absolute Antibody), Daclizumab (Absolute Antibody)) were added at 50 μg/ml (mouse) and 10 μg/ml (human), respectively, and were incubated with the cells for 30 mins at 37°C, following which cells were stimulated with IL-2 (50U/ml (mouse) and 10 U/ml (human) respectively, both Peprotech) for 10 mins at 37°C. IL-2 induced STAT5 phosphorylation was stopped when the cells were fixed and permeabilized with the eBioscience™ FoxP3 / Transcription Factor Staining Buffer Set and treated with the BD Phosflow Perm Buffer III. Blocking was calculated as follows: %

Europe PMC Funders Author Manuscripts

blocking = 100 x [(% Stat5$^+$ cells No Ab group - % Stat5$^+$ cells 50ug/ml Ab group) / (% Stat5$^+$ cells No Ab group)].

X-ray crystallography: Protein preparation, crystallization, structure determination

A complex out of deglycosylated human CD25 (SinoBiological) and Fab of RG6292 was formed and crystallized. Lyophilized human CD25 was dissolved in Milli-Q water to a final concentration of 1mg/ml. Endoproteinase Glu-C (Hampton Research) was added in a molar ratio of 1:10 and the mix incubated for 2 hours at 37°C. The reaction was stopped by addition of diisopropyl fluorophosphate (1:10). Subsequently, the protein was deglycosylated for 4 hours at 22°C with 40 U/μg N-glycosidase F (PNGase F, New England Biolabs). The Fab fragment of RG6292 was added to the deglycosylated CD25 in a molar ratio of 1,1:1. Complex formation was completed within one hour at 22°C. Prior to crystallization, the protein complex was concentrated to 11.2 mg/ml and centrifuged at 20,000g. Crystallization droplets were set up at 21°C by mixing 0.1μl of protein solution with 0.1μl crystallization screen solution (BCS Screen, Molecular Dimensions). Crystals appeared after 120 days out of 25% v/v PEG Smear Medium (12.5% w/v PEG 3350, 12.5% w/v PEG 4000, 12.5% w/v PEG 2000, 12.5% w/v PEG 5000 MME) and 0.1 M sodium acetate pH 4.5. For data collection, crystals were transferred to crystallization solution supplemented with 20% glycerol and cryo-cooled in liquid nitrogen. X-ray diffraction data were collected at a wavelength of 0.99982 Å using a Pilatus 6M detector at the beamline X10SA of the Swiss Light Source (Villigen, Switzerland).

Data has been processed with XDS[43] and scaled with SADABS (BRUKER). The monoclinic crystals belong to the space group P21 with cell axes of a= 51.38 Å, b= 44.32 Å, c= 140.08 Å, β= 92.41° and diffract to a resolution of 1.83 Å. The structure was determined by molecular replacement with the program PHASER[44] using the coordinates of an in house Fab fragment as search model in combination with the coordinates of CD25 taken from PDB entry 2B5I. With programs from the CCP4 suite[45] and BUSTER[46], the initial coordinates obtained by molecular replacement were subsequently refined by rigid body and positional refinement. Difference electron density was used to exchange amino acid residues different to the search model. Manual rebuilding of protein was done with COOT[47]. The asymmetric unit is assembled out of one CD25 Fab RG6292 complex molecule. All graphical presentations were prepared with PYMOL (The PyMOL Molecular Graphics System, Version 2.3.1. Schrödinger, LLC.). Data collection and refinement statistics are summarized in Supplemental Table 1. Coordinates and structure factors have been deposited with the Protein Data Bank (accession code 6YIO).

Binding experiments

To quantify binding of αCD25^{NIB}, splenocytes were isolated of spleens resected from female C57BL/6-Foxp3tm1Flv/J mice as described above. For binding experiments with RG6292 and Daclizumab, SU-DHL1 tumor cells (human CD25$^+$) and HSC-F cells (cynomolgus CD25$^+$) were used. Briefly, cells were incubated with indicated serial dilutions of test antibody for 1 hour at 4°C followed by repeated washing with ice-cold PBS (Gibco) containing 0.1% BSA (Sigma). For detection of bound test antibody, samples were stained for 30 minutes at 4°C with FITC labeled secondary antibody against human and mouse Fcγ,

respectively (both Jackson Laboratories). Samples were stained with LIVE/DEAD™ fixable Aqua Dead Cell Stain Kit (ThermoFisher). Living mouse Treg cells ($Aqua^-$, $mRFP^+$ singlets) and tumor cells ($Aqua^-$, singlets), respectively, were gated and the mean fluorescence intensity of the secondary antibody was determined.

ADCC, ADCP, T cell activation assay and cytotoxicity assay

Human PBMC were isolated from buffy coats of healthy donors (Zurich blood donation center in accordance with the Declaration of Helsinki) using standard density-gradient isolation over Histopaque-1077 (Sigma-Aldrich). NK cells were isolated there-off using the MACS human NK cell isolation kit (Miltenyi Biotec) followed by overnight activation in RPMI 1640 medium (Gibco) containing 10% FCS (Gibco), 1% Glutamax (Invitrogen/Gibco) and human recombinant IL-2 (2 ng/ml, Peprotech). $CD14^+$ monocytes were isolated from human PBMC using MACS human CD14 micro beads (Miltenyi Biotec) followed by M2 macrophage differentiation for 5 days in complete RPMI 1640 medium (Gibco) containing recombinant macrophage colony stimulating factor (M-CSF) (50 ng/ml, Peprotech). Purity of M2 differentiation was confirmed using a staining antibody cocktail against human CD3, CD14, CD16, CD32a, CD32b, CD64, CD80, CD163, CD206 and CD38. iTregs were differentiated from naïve CD4 T cells by activation with Dynabeads® Human T-Activator CD3/CD28 ($1*10^6$ beads/ ml, bead to cell ratio 1:1, Gibco) for 5-7 days in iTreg media comprised of X-Vivo 15 (Lonza) supplemented with 10% FCS (Gibco), 1% Glutamax (Invitrogen/Gibco), N-acetylcysteine (2 mg/ml, Sigma), Na-Pyruvate (1x, Gibco), Hepes (1x, Gibco), NEAA (1x, Gibco), Pen/Strep (1x, Gibco), 2-mercaptoethanol (50 μM), Thermo Fischer scientific), Proleukin/Aldesleukin (300 U/ml, Novartis), Rapamycin (100 ng/ml, Sigma) and rhTGFβ1 (10 ng/ml, Miltenyi Biotec). Naïve CD4 T cells were isolated from human PBMC using the MACS human naïve CD4 T cell isolation kit II (Miltenyi Biotec). Purity of iTreg generation was confirmed using a staining antibody cocktail against human CD3, CD4, CD25 and FoxP3. iTregs were labelled with the PKH26 cell linker kit (Sigma) for easy flow cytometric cell detection in ADCC and ADCP assays.

For ADCP evaluation, 10,000 donor matched, PKH26 labeled iTregs and 100,000 M2 macrophages were plated in RPMI 1640 medium (Gibco) containing 2% FCS (Gibco) and 1% Glutamax (Invitrogen/Gibco). A serial dilution row of RG6292, the fully fucosylated RG6292, and an a-fucosylated human IgG1 isotype control antibody were added at a starting concentration of 0.1 μg/ml. After 4 hours of incubation at 37°C, samples were stained with LIVE/DEAD™ fixable Aqua Dead Cell Stain Kit (ThermoFisher) and anti-human CD14 (M5E2) in the presence of human Fc Block (BD). For normalization, CountBright absolute counting beads (ThermoFisher) were added. The phagocytosis was calculated in percent as 100 * count of phagocytosed iTreg ($PKh26^+CD14^+$) divided by count of total iTreg (total $PkH26^+$).

For ADCC evaluation, 20,000 PKH26 labeled iTregs and 100,000 IL-2 conditioned NK cells were plated in RPMI 1640 medium (Gibco) containing 10% FCS (Gibco) and 1% Glutamax (Invitrogen/Gibco). A tenfold serial dilution row of RG6292 ($\alpha CD25^{NIB}$ GlymaxX), the fully fucosylated RG6292, an a-fucosylated human IgG1 isotype control antibody and Daclizumab (IgG1) were added at a starting concentration of 10 μg/ml and incubated with

the cells for 4 hours at 37°C. Samples were stained with LIVE/DEAD™ fixable Aqua Dead Cell Stain Kit (ThermoFisher) and anti-human CD134 (Ber-Act35), CD25 (2A3), CD69 (FN50) and CD56 (5.1H11). Living iTreg cells were gated (Aqua$^-$, PkH-26$^+$) and percentage of positive cells were used to calculate specific lysis.

To prove that RG6292 was not interfering with IL-2 signaling during T cell activation, human Pan T cells (Allcell, Caltag Medsystems) were activated with Dynabeads Human T-Activator CD3/CD28 (ThermoFisher) for 3 days in the presence of RG6292, a human IgG1 isotype control antibody, Daclizumab (IgG1) and an IL-2 neutralizing antibody, all at a concentration of 10 μg/ml. The assay media was RPMI 1640 medium (Gibco) containing 10% FCS (Gibco). Samples were stained with Fixable Viability Dye eFluor™ 780 (ThermoFisher) and anti-human CD3 (UCHT1), CD4 (SK3), CD8 (RPA-T8), Ki67 and Granzyme B (GB11). Living CD4$^+$ and CD8$^+$ T cells were analyzed for Granzyme B and Ki67 expression.

The combined ADCP and ADCC potency of RG6292 and its differential effect on activated CD8$^+$ T cells versus Treg cells was tested on polyclonally activated human PBMC. CFSE labelled (50 nM, Sigma-Aldrich) human PBMC were activated for 72 hours on irradiated NIH/3T3 fibroblasts using Anti-Biotin MACSiBead (Miltenyi Biotec) coated with biotinylated anti-human CD3 antibody (30 μg protein per 1*10^6 beads, clone OKT3, Miltenyi Biotec, 1 bead per cell) in the presence of a serial dilution row of RG6292 (αCD25^{NIB} GlymaxX), or a human IgG1 Isotype Control (BioLegend). Samples were stained with LIVE/DEAD™ fixable Aqua Dead Cell Stain Kit (ThermoFisher) and fluorescent dye-conjugated antibodies anti-human CD8 (RPA-T8), CD4 (OKT4), NKp46 (9E2), CD25 (2A3) and CD69 (FN50). For FoxP3 detection cells were stained using the FoxP3 Transcription Factor Staining Buffer Set (eBioscience) and the anti-human FoxP3 antibody (206D). Treg (CD4$^+$, CD25$^+$ FoxP3$^+$CFSE^{high}), activated CD4 (CD4$^+$ FoxP3$^-$ CD69$^+$) and activated CD8 T cells (CD8$^+$, CD69$^+$) were gated, absolute counts determined based on reference beads and lysis relative to blank sample calculated.

Determination of binding properties of surrogate murine αCD25-antibodies by SPR-experiments

His-tagged murine CD25 antigen 50292-M08H was purchased from Sino Biological.

All SPR experiments were performed on a BIAcore© B2000 instrument (GE Healthcare) at 25°C and sample compartment was set to 16°C. Measurement of apparent Kd of binding surrogate murine antibodies αCD25^{NIB} and αCD25^{PC61} to recombinant mouse CD25 (Sino Biological 50292-M08H) was determined using the dextran-based carboxymethylated sensor chip CM5. For capturing the αCD25-antibodies on the chip, an anti-mouse antibody (30 μg/ml pH 5.0) was covalently bound for 10 minutes to the NHS/EDC activated CM5 surface to an immobilization level of about 16000 RU. In the next step, the murine αCD25-antibodies were captured to a level of about 140 RU. Association of murine CD25 antigen (Sino Biologicial 50292-M08H) at concentrations of 3.13, 6.25, 12.5, 25, 50, 100, 200, 400 and 800 nM to the captured murine surrogate CD25-antibodies was recorded for 360 seconds and dissociation for 600 seconds at a flow rate of 25 μl/min in kinetics buffer consisting of 10 mM HEPES pH 7.4, 150 mM NaCl, 3 mM EDTA, 0.05% Tween 20.

Regeneration of the sensor chip surface between each cycle was performed by washing the chip with 10 mM glycine pH 1.7 at a flow rate of 25 μl/min. Apparent Kd values were calculated using the bivalent analyte fitting model (Biacore evaluation software).

Human Tumor Samples

The dissociated frozen human tumor samples (DTC) were obtained from Conversant Bio (USA) and preparation of DTCs was previously described in[48]. The lung cancer sample was derived from a 68-year-old, non-Hispanic white male diagnosed with lung adenocarcinoma (overall clinical stage III-B). The colorectal cancer sample was derived from a 55 year old, non-Hispanic white female diagnosed with colorectal adenocarcinoma (overall clinical stage II-A). DTCs and IL-2 activated allogenic NK cells were co-incubated in the presence of 10μg/mL RG6292 (αCD25^{NIB} GlymaxX, fully fucosylated or Fc silent) for 3 hours at an effector to target ratio of 10 to 1 in complete RPMI media. Samples were stained with Fixable Viability Stain 510 (BD Horizon) and fluorescent dye-conjugated antibodies anti-human CD45 (HI30), CD3 (UCHT1), CD8 (RPA-T8), CD4 (SK3), CD45RA (EBA-1), CD127 (HIL-7R-M21), CD14 (M5E2), CD56 (NCAM16.2) and EpCAM (9C4). For FoxP3 detection, cells were stained using the FoxP3 Transcription Factor Staining Buffer Set (eBioscience) and the anti-human FoxP3 antibody (236A/E7). Treg (EpCAM^{-} CD45^{+} CD56^{-} CD3^{+} CD4^{+}, CD127^{low} FoxP3^{+}) and CD8 T cells (EpCAM^{-} CD45^{+} CD56^{-} CD3^{+} CD8^{+}) counts were analyzed by flow cytometry.

Statement on Patient consent

All Discovery Life Sciences samples are ethically obtained, following all applicable HHS/OHRP, ISBER, and NCI/BBRB regulations, guidelines and best practices, as well as all other relevant FDA, state statutory requirements and international guidelines including compliance with patient privacy regulations.

4-week toxicity study in cynomolgus monkey: H&E nasal cavity

αCD25 was tested in a 4-week repeat dose toxicity study in cynomolgus monkeys at 10, 30 and 100 mg/kg/dose Q2W by 30-minute peripheral intravenous infusion via tail vein. The study was performed in accordance with the U.S. Department of Health and Human Services, Food and Drug Administration, United States Code of Federal Regulations, Title 21, Part 58: Good Laboratory Practice for Nonclinical Laboratory Studies and as accepted by Regulatory Authorities throughout the European Union (OECD Principles of Good Laboratory Practice) and Japan (MHLW). A complete tissue set was collected for histopathologic examination. Tissue samples were fixed in 10% neutral buffered formalin, paraffin embedded, sectioned at 5 μm, stained with hematoxylin–eosin (H&E), and evaluated by a board certified veterinary pathologist with a standard light microscope.

Flow cytometry

Acquisition was performed with a FACSymphony and FACS Fortessa (both BD Biosciences). Data analysis was performed in FlowJo version 10.5.3 (Tree Star Inc.). Directly conjugated antibodies employed for flow cytometry are listed in Supplementary table 6. Cross titration confirmed that CD25 gating and Treg detection was not compromised

by competition between drug and detection antibody. Intranuclear staining of FoxP3 and Ki67 was performed using the FoxP3 Transcription Factor Staining Buffer Set (eBioscience). For quantification of absolute number of cells, a defined number of fluorescent beads (Cell Sorting Set-up Beads for UV Lasers, ThermoFisher) was added to each sample before acquisition and used as a counting reference.

For pSTAT5 staining, TILs/LN/splenocytes/PBMCs were rested for 2 hours in FCS-free media followed by 10 min stimulation with IL-2 (Peprotech) and fixed for 30 min with Fixation/Permeabilization buffer (ThermoFisher) and Perm Buffer III (BD Phosphlow) followed by the staining.

Analysis of flow cytometry data

FCS files were imported using flowCore and logicle transform applied using the estimateLogicle function. UMAP dimension reduction was carried out with the uwot package[49], the plot represent models trained with all available data. Samples with over 1000 live pre-gated events (resulting in the exclusion of one sample from a mouse treated with anti-CD25 alone) were subjected to unsupervised clustering. Data were clustered onto a 7x7 node square self-organizing map (SOM) implemented in the FlowSOM package[50]. This was followed by high resolution clustering of nodes into 20 subpopulations by hierarchical consensus clustering with the ConsensusClusterPlus package, to ensure homogeneity of individual groups as described[51]. To determine differential abundance of clusters between conditions, we applied negative binomial generalized linear models using the package edgeR as recently described for cytometry data[52].

Data analysis

Data analysis was performed in FlowJo version 10.5.3 (Tree Star Inc.). Statistical analyses were performed in Prism 7 (GraphPad Software, Inc.); p values were calculated using one or two-way ANOVA with Tukey post-tests (ns=$p>0.05$, *$p<0.05$, **$p<0.01$, ***$p<0.001$, ****$p<0.0001$). Analysis of Kaplan-Meier survival curves was done with two-sided log-rank test. EC50 values were performed in Prism 7 (GraphPad Software, Inc.) using the inbuilt non-linear regression curve fit (log (agonist) vs response, variable slope, 4 parameter).

All the data presented has been reviewed by a statistician to ensure scientific rigor and diligence of our data.

Further information on research design is available in the Nature Research Reporting Summary linked to this article.

Europe PMC Funders Author Manuscripts

Extended Data

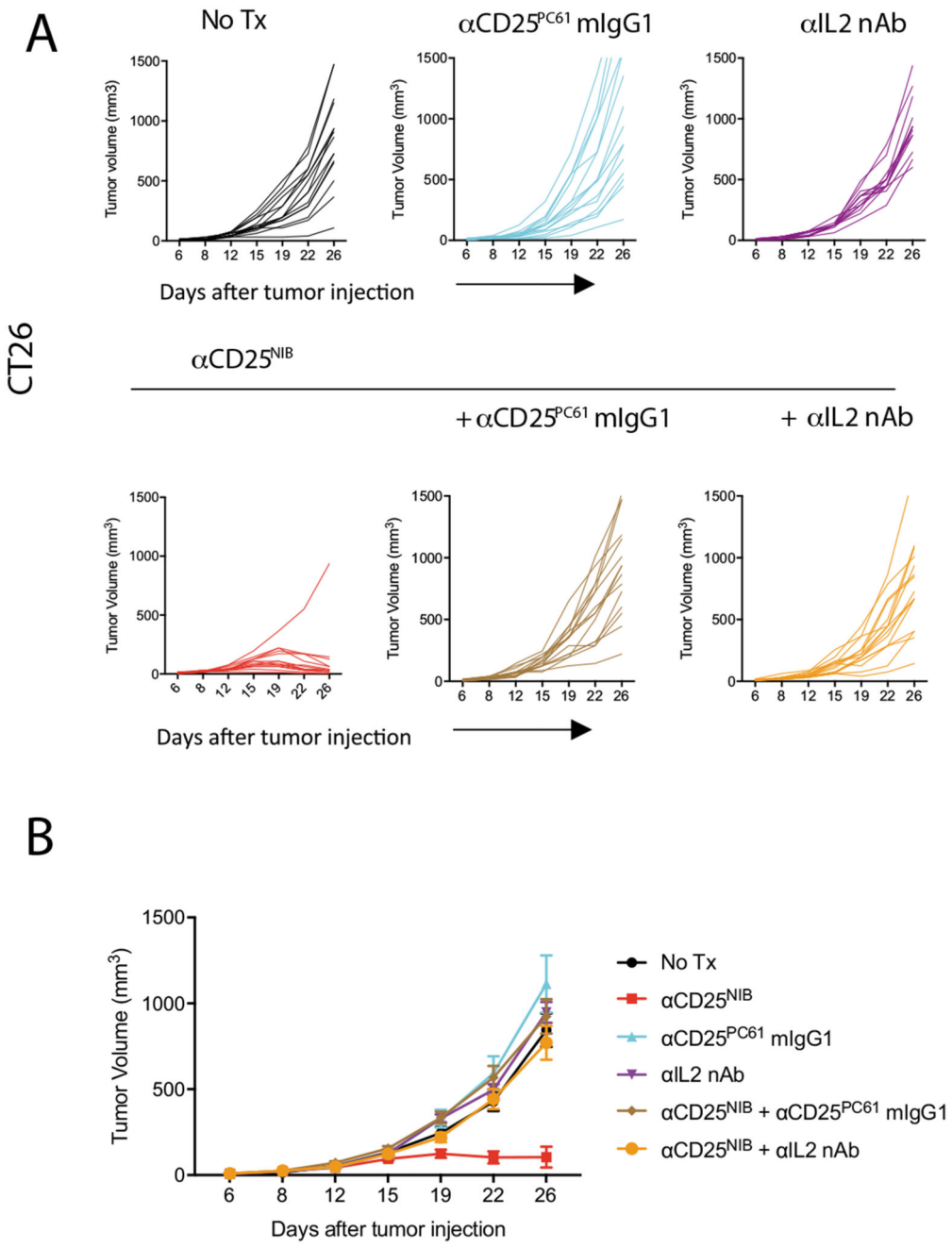

Extended Data Fig. 1. αCD25^{NIB} promotes single dose, single agent activity against established tumors

(A) Balb/C mice were injected with 500,000 CT26 tumor cells. Treatment was started on day 6 post-tumor inoculation. **(B)** Mean tumor volume of the tumor-bearing mice in **(A)**, n=10 mice/group. Data are presented as mean values +-SEM.

Europe PMC Funders Author Manuscripts

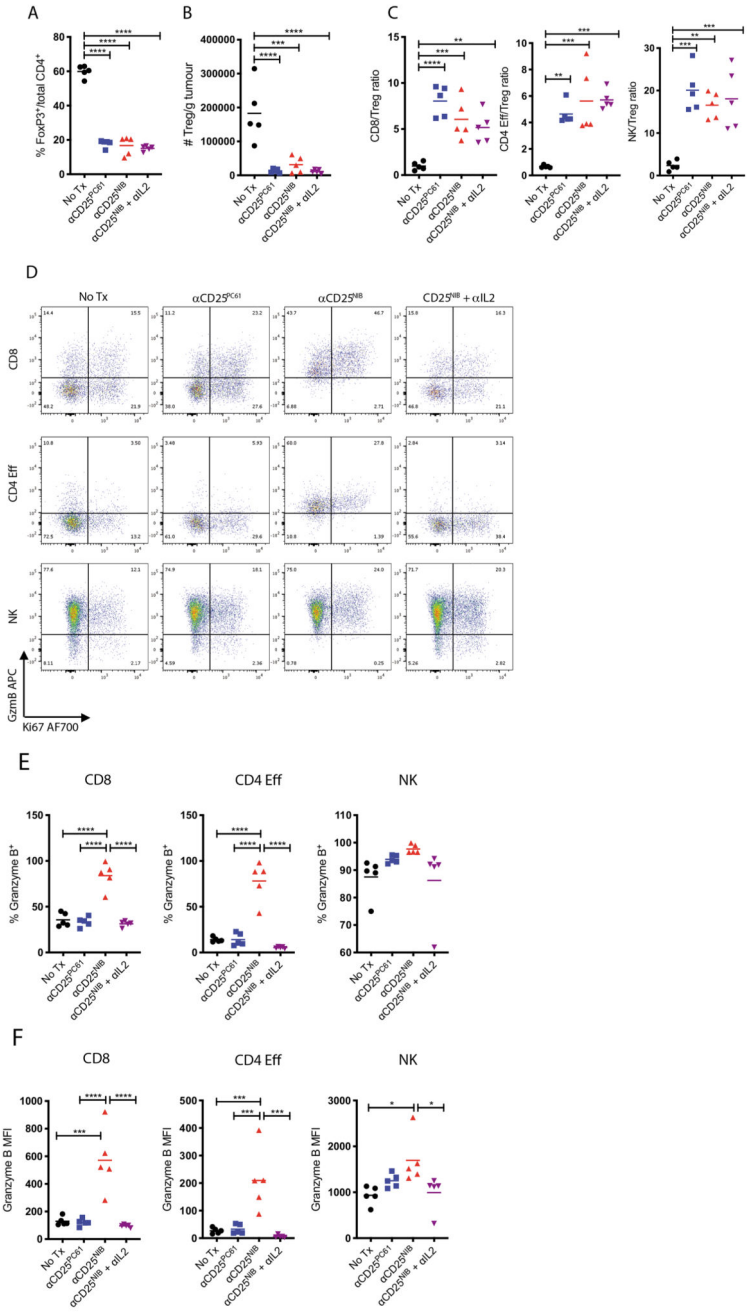

Extended Data Fig. 2. αCD25^{NIB} depletes Tregs and drives effector immune responses.

C57BL6 mice were injected with 500,000 MC38 tumor cells. Once tumors were palpable, on day 7, mice were injected IP with αPC61/αCD25^{NIB}/αCD25^{NIB} + αIL2 (200μg). Tumors and LN were harvested on day 15 post-tumor inoculation and processed as described in materials and methods section. **(A)** Graph showing % FoxP3^{+} cells of total CD4^{+} cells. **(B)** Absolute number of Tregs shown as number of Tregs/g of tumor. p-value=0.0003 between No Tx and αCD25^{NIB} group. ****=p-value <0.0001 **(C)** Ratio of effector T cells over Tregs. For CD8/Treg ratio, P-value between No tx versus

αCD25^{NIB}=0.0008, and between No tx and αCD25^{NIB} + αIL2 =0.0045. For CD4 Eff/Treg ratio, p-value between no tx and /αCD25^{PC61} = 0.0056, between No tx and αCD25^{NIB}=0.0002, between no tx and αCD25^{NIB} + αIL2=0.0001. For NK/Treg ratio, p-value=0.0001 for no tx versus αCD25^{PC61}, 0.0010 for no tx versus αCD25^{NIB} and 0.0004 for No tx versus αCD25^{NIB} + αIL2. **(D)** Representative FACS plots showing Granzyme B expression versus Ki67 expression in CD8, CD4 effectors and NK cells. **(E)** Graph showing percentage of Granzyme B^{+} cells in different effector subsets. **(F)** Graph showing the Mean Fluorescence Intensity of Granzyme of the effector cells plotted in **(E)**. For CD8 cells, p-value between No tx group and αCD25^{NIB} =0.0001. For CD4 Eff, p-values between No tx versus αCD25^{NIB} =0.0007, for αCD25^{NIB} versus αCD25^{PC61}=0.0009, and between αCD25^{NIB} and αCD25^{NIB} + αIL2 group= 0.0002. For NK cells, p-value between No tx group and αCD25^{NIB} group=0.0164 and between αCD25^{NIB} and αCD25^{NIB} + αIL2 group=0.0280. Quantification plots: mean ± SEM, 1-way ANOVA, Tukey's multiple comparisons test (ns=p>0.05, *p<0.05, **p<0.01, ***p<0.001, ****p<0.0001).

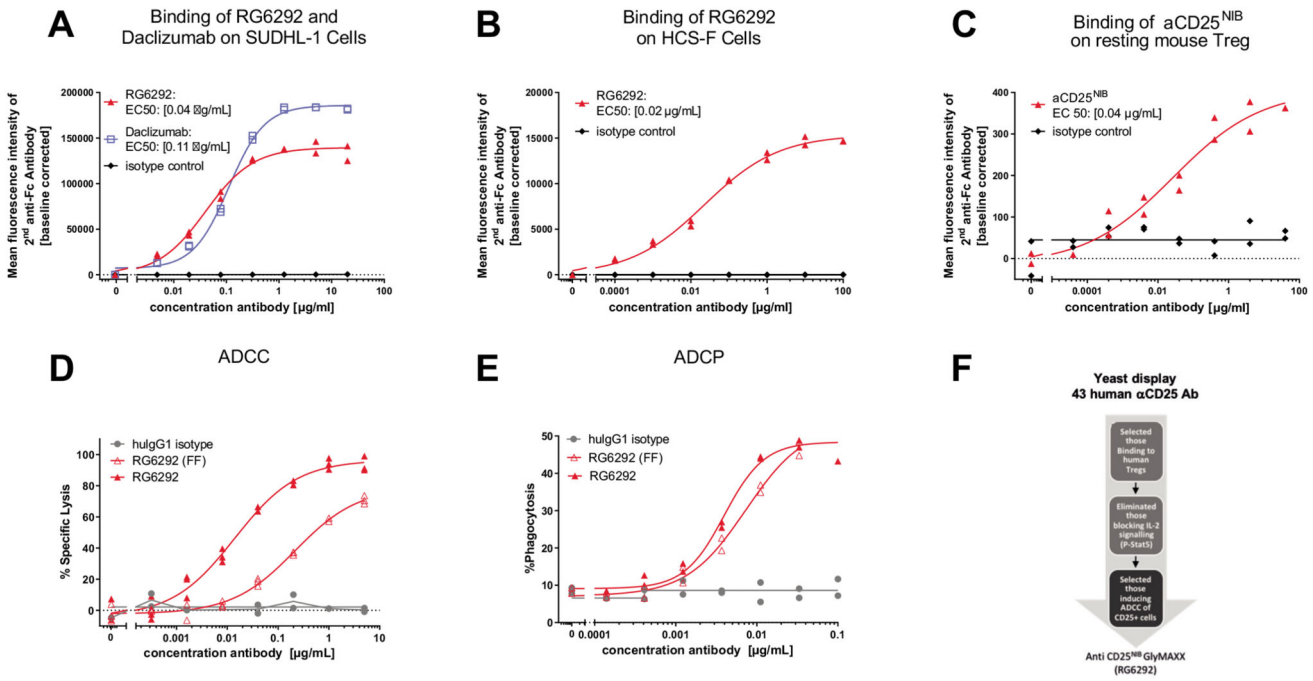

Extended Data Fig. 3. Binding of αCD25^{NIB}, RG6292 and Daclizumab to mouse, human and cynomolgus CD25 positive cells. ADCC and ADCP capacity of RG6292.

For binding experiments with RG6292 and Daclizumab, SU-DHL1 tumor cells (human CD25^{+}, **(A)**) and HSC-F cells (cynomolgus CD25^{+}, **(B)**) were used. To quantify binding of αCD25^{NIB}, splenocytes were isolated of spleens resected from female C57BL/6-Foxp3tm1Flv/J mice **(C)** Cells were incubated with indicated serial dilutions of the test antibody detected then by fluorescently labeled 2nd antibody against human and mouse Fcγ, respectively. Living mouse Treg cells (Aqua^{-}, mRFP^{+} singlets) and tumor cells (Aqua^{-}, singlets), respectively, were gated and the mean fluorescence intensity of the secondary antibody was plotted. EC50 values were calculated by as described in the data analysis

Europe PMC Funders Author Manuscripts

section in materials and methods. Shown are technical duplicates of one representative experiment out of several independent ones conducted (N>2). **(D)** RG6292 (and the fully fucosylated version RG6292 (FF)) depleted via ADCC *in-vitro* differentiated Treg cells using purified, IL-2 activated NK cells. Shown are technical duplicates of one representative experiment out of several independent ones conducted (N>2). **(E)** RG6292 and RG6292 (FF) mediated ADCP of *in-vitro* differentiated Treg cells when co-cultured with MCSF differentiated macrophages. Flow cytometric analysis was performed to determine percentage of phagocytosis. Shown are technical duplicates of one representative experiment out of several independent ones conducted (N>2). **(F)** Schematics of binder selection.

Europe PMC Funders Author Manuscripts

Europe PMC Funders Author Manuscripts

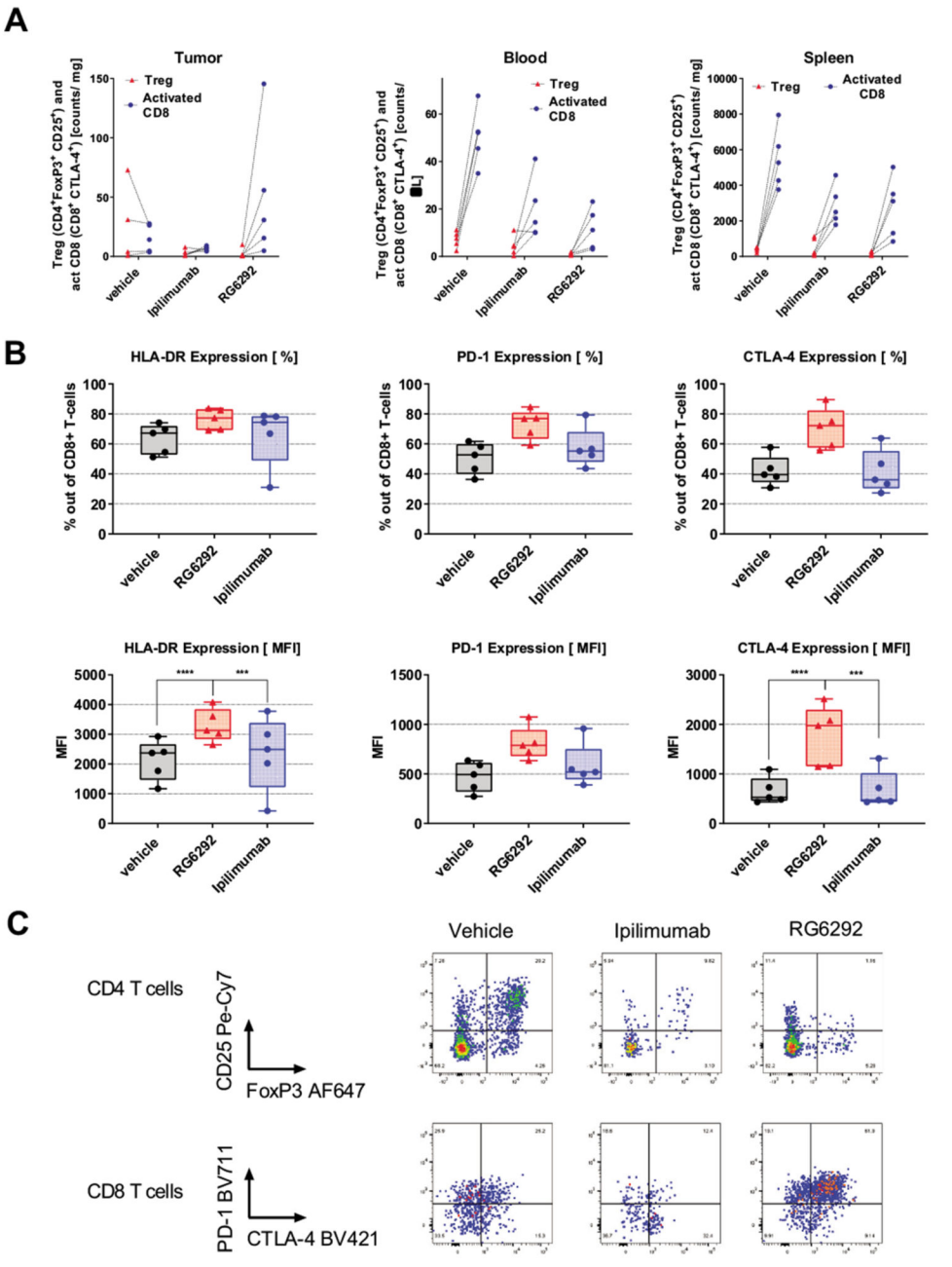

Extended Data Fig. 4. Anti-human-CD25^{NIB} (RG6292) depletes Treg and drives T cell activation in tumor-bearing humanized mice.

Stem cell humanized female NOG mice bearing an established s.c. BxPC-3 tumor were injected i.p. with vehicle, RG6292 [4 mg/kg] or Ipilimumab [10 mg/kg]. After 72 hrs, splenocytes, blood lymphocytes and tumor infiltrating lymphocytes were isolated and evaluated for counts of activated CD8$^+$ T cells (huCD45$^+$, huCD3$^+$, huCD8$^+$ huCTLA-4$^+$) and Tregs (huCD45$^+$, huCD3$^+$, huCD4$^+$, huFoxP3$^+$) as well as for markers of recent T cell activation. **(A)** Ipilimumab as well as RG6292 decreased the intratumoral Treg counts. An

increase of intratumoral activated $CD8^+$ T cell count was only evident after administration of RG6292. Normalized counts were plotted for the respective treatment groups. Each symbol represents one animal (n=5 mice), CD8 and Treg cells are connected for the same animals **(B)** Intratumoral $CD8^+$ T cells after RG6292 treatment were highly activated and had increased levels of HLA-DR, PD-1 and CTLA-4 (MFI as well as % of positive cells). Each symbol represents one animal (n=5 mice). The box and whiskers plots show minima and maxima and the median. Statistical analysis of RG6292 and Ipilimumab treated groups against vehicle group is indicated. Data was analyzed using 2-way ANOVA, Dunnet's multiple comparisons test (ns=p>0.05, *p<0.05, **p<0.01, ***p<0.001, ****p<0.0001) (p-value between RG6292 and Ipilimumab was 0.0001 for CTLA4 MFI on CD8 T cells and 0.0008 for HLA-DR on CD8 T cells. **(C)** Representative FACS plots showing CD25 expression versus FoxP3 expression in $CD4^+$ T cells and PD-1 expression versus CTLA-4 expression in $CD8^+$ T cells for vehicle, RG6292 and Ipilimumab treated animals.

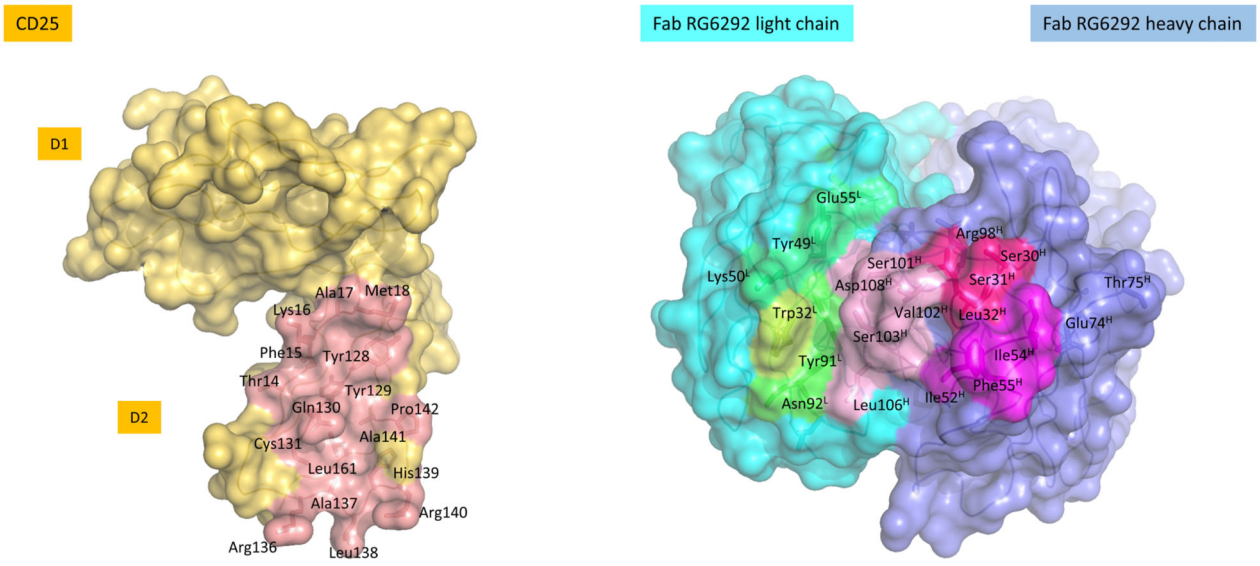

Extended Data Fig. 5. Open-book representation of the interaction site between CD25 and Fab RG6292.

CD25 shown as surface colored in yellow with residues contributing to the interface highlighted in salmon. Fab light and heavy chain are colored in cyan and blue. Residues from the heavy chain CDR1, CDR2 and CDR3 contributing to the interface are labeled and the surface colored in dark pink, magenta and light pink, respectively. Light chain residues of CDR1 to 3 contributing to the interface are labeled and shown in yellow, lime green and green, respectively.

Supplementary Material

Refer to Web version on PubMed Central for supplementary material.

Acknowledgments

S.A.Q. is funded by a Cancer Research U.K. (CRUK) Senior Cancer Research Fellowship (C36463/A22246) and a CRUK Biotherapeutic Program Grant (C36463/A20764). K.S.P. receives funding from the NIHRBTRU for Stem Cells and Immunotherapies (167097), of which he is the Scientific Director. This work was undertaken at UCL with support from the CRUK-UCL Centre (C416/A18088), the Cancer Immuno-therapy Accelerator Award (CITA-CRUK) (C33499/A20265), and CRUK funding schemes for National Institute for Health Research Biomedical Research Centres and Experimental Cancer Medicine Centres. The authors would like to thank Prof. Thomas Singer for the guidance provided on the non-clinical safety assessment of RG6292.

Data Availability Statement

The datasets generated during and/or analysed during the current study are available from the corresponding author on reasonable request. Crystal structure coordinates and structure factors have been deposited with the Protein Data Bank under accession code 6YIO.

References

1. Plitas G, Rudensky AY. Regulatory T cells: Differentiation and function. Cancer Immunol Res. 2016; 4:721–725. [PubMed: 27590281]
2. Elpek KG, Lacelle C, Singh NP, Yolcu ES, Shirwan H. CD4 + CD25 + T Regulatory Cells Dominate Multiple Immune Evasion Mechanisms in Early but Not Late Phases of Tumor Development in a B Cell Lymphoma Model. J Immunol. 2007; 178:6840–6848. [PubMed: 17513732]
3. Golgher D, Jones E, Powrie F, Elliott T, Gallimore A. Depletion of CD25+ regulatory cells uncovers immune responses to shared murine tumor rejection antigens. Eur J Immunol. 2002; 32:3267–3275. [PubMed: 12555672]
4. Jones E, et al. Depletion of CD25+ regulatory cells results in suppression of melanomagrowth and induction of autoreactivity in mice. Cancer Immun. 2002
5. Onizuka S, et al. Tumor rejection by in vivo administration of anti-CD25 (interleukin-2 receptor α) monoclonal antibody. Cancer Res. 1999
6. Quezada SA, Peggs KS, Curran MA, Allison JP. CTLA4 blockade and GM-CSF combination immunotherapy alters the intratumor balance of effector and regulatory T cells. J Clin Invest. 2006; doi: 10.1172/JCI27745
7. Mihm MC, et al. Immunologic and clinical effects of antibody blockade of cytotoxic T lymphocyte-associated antigen 4 in previously vaccinated cancer patients. Proc Natl Acad Sci. 2008; doi: 10.1073/pnas.0712237105
8. Simpson TR, et al. Fc-dependent depletion of tumor-infiltrating regulatory T cells co-defines the efficacy of anti-CTLA-4 therapy against melanoma. J Exp Med. 2013; doi: 10.1084/jem.20130579
9. Wilson NS, et al. Activating Fc γ receptors contribute to the antitumor activities of immunoregulatory receptor-targeting antibodies. J Exp Med. 2013; 210:1685–1693. [PubMed: 23897982]
10. Selby MJ, et al. Anti-CTLA-4 Antibodies of IgG2a Isotype Enhance Antitumor Activity through Reduction of Intratumoral Regulatory T Cells. 2013; 1:32–43.
11. Sharma A, et al. Anti-CTLA-4 immunotherapy does not deplete Foxp3 Þ regulatory T cells (Tregs) in human cancers. Clin Cancer Res. 2019; 25:1233–1238. [PubMed: 30054281]
12. Vargas FA, et al. Fc Effector Function Contributes to the Activity of Human Anti-CTLA-4 Antibodies. Cancer Cell. 2018; 33:649–663.e4. [PubMed: 29576375]
13. Waight JD, et al. Selective FcγR Co-engagement on APCs Modulates the Activity of Therapeutic Antibodies Targeting T Cell Antigens. Cancer Cell. 2018; 33:1033–1047.e5. [PubMed: 29894690]
14. Ha D, et al. Differential control of human Treg and effector T cells in tumor immunity by Fc-engineered anti–CTLA-4 antibody. Proc Natl Acad Sci U S A. 2019; 116:609–618. [PubMed: 30587582]

15. Chevrier S, et al. An Immune Atlas of Clear Cell Renal Cell Carcinoma. Cell. 2017; 169:736–749.e18. [PubMed: 28475899]
16. Azizi E, et al. Single-Cell Map of Diverse Immune Phenotypes in the Breast Tumor Microenvironment Resource Single-Cell Map of Diverse Immune Phenotypes in the Breast Tumor Microenvironment. Cell. 2018; :1293–1308. DOI: 10.1016/j.cell.2018.05.060
17. Vargas FA, et al. Fc-Optimized Anti-CD25 Depletes Tumor-Infiltrating Regulatory T Cells and Synergizes with PD-1 Blockade to Eradicate Established Tumors. Immunity. 2017; 46:577–586. [PubMed: 28410988]
18. Kapic E, Becic F, Kusturica J. Basiliximab, mechanism of action and pharmacological properties. Med Arh. 2004
19. Baldassari LE, Rose JW. Daclizumab: Development, Clinical Trials, and Practical Aspects of Use in Multiple Sclerosis. Neurotherapeutics. 2017; doi: 10.1007/s13311-017-0553-8
20. Moreau J-L, et al. Monoclonal antibodies identify three epitope clusters on the mouse p55 subunit of the interleukin 2 receptor: relationship to the interleukin 2-binding site. Eur J Immunol. 1987; doi: 10.1002/eji.1830170706
21. Spolski R, Li P, Leonard WJ. Biology and regulation of IL-2: from molecular mechanisms to human therapy. Nat Rev Immunol. 2018; 18:648–659. [PubMed: 30089912]
22. Arenas-ramirez N, Woytschak J. Interleukin-2 : Biology, Design and Application. Trends Immunol. 2015; 36:763–777. [PubMed: 26572555]
23. Liao W, Lin JX, Leonard WJ. Interleukin-2 at the Crossroads of Effector Responses, Tolerance, and Immunotherapy. Immunity. 2013; 38:13–25. [PubMed: 23352221]
24. Scheffold A, Murphy KM, Höfer T. Competition for cytokines : T reg cells take all. Nat Immunol. 2007; 8:1285–1287. [PubMed: 18026078]
25. Kohm AP, Miller SD. Response to Comment on “Cutting Edge: Anti-CD25 Monoclonal Antibody Injection Results in the Functional Inactivation, Not Depletion, of CD4 + CD25 + T Regulatory Cells”. J Immunol. 2006; 177:2037–2038.
26. Malek TR, Castro I. Interleukin-2 Receptor Signaling: At the Interface between Tolerance and Immunity. Immunity. 2010; 33:153–165. [PubMed: 20732639]
27. Van Elsas A, et al. Elucidating the autoimmune and antitumor effector mechanisms of a treatment based on cytotoxic T lymphocyte antigen-4 blockade in combination with a B16 melanoma vaccine: Comparison of prophylaxis and therapy. J Exp Med. 2001; doi: 10.1084/jem.194.4.481
28. Hashimoto M, et al. CD8 T Cell Exhaustion in Chronic Infection and Cancer: Opportunities for Interventions. Annu Rev Med. 2018; doi: 10.1146/annurev-med-012017-043208
29. Blank CU, et al. Defining ‘T cell exhaustion’. Nat Rev Immunol. 2019; doi: 10.1038/s41577-019-0221-9
30. Bulliard Y, et al. OX40 engagement depletes intratumoral Tregs via activating FcγRs, leading to antitumor efficacy. Immunol Cell Biol. 2014; doi: 10.1038/icb.2014.26
31. Wolchok JD, et al. Fc-dependent depletion of tumor-infiltrating regulatory T cells co-defines the efficacy of anti–CTLA-4 therapy against melanoma. J Exp Med. 2013; doi: 10.1084/jem.20130579
32. Furness AJS, Vargas FA, Peggs KS, Quezada SA. Impact of tumour microenvironment and Fc receptors on the activity of immunomodulatory antibodies. Trends in Immunology. 2014; doi: 10.1016/j.it.2014.05.002
33. Das R, et al. Combination Therapy with Anti–CTLA-4 and Anti–PD-1 Leads to Distinct Immunologic Changes In Vivo. J Immunol. 2015; doi: 10.4049/jimmunol.1401686
34. National Cancer Institute. [Accessed: 31st October 2019] First-In-Human Study of Monoclonal Antibody BMS-986218 by Itself and in Combination With Nivolumab in Patients With Advanced Solid Tumors. Clinical Trials. 2019. Available at: https://www.cancer.gov/about-cancer/treatment/clinical-trials/search/v?id=NCI-2017-00920&r=1
35. Guo H, et al. Structural Basis for the Blockage of IL-2 Signaling by Therapeutic Antibody Basiliximab. J Immunol. 2009; doi: 10.4049/jimmunol.0903178
36. Simpson TR, et al. Fc-dependent depletion of tumor-infiltrating regulatory t cells codefines the efficacy of anti-CTLA-4 therapy against melanoma. J Exp Med. 2013; doi: 10.1084/jem.20130579

37. Kim JM, Rasmussen JP, Rudensky AY. Regulatory T cells prevent catastrophic autoimmunity throughout the lifespan of mice. Nat Immunol. 2007; doi: 10.1038/ni1428
38. Wang X, Rickert M, Garcia KC. Structure of the quaternary complex of interleukin-2 with its alpha, beta, and gammac receptors. Science. 2005; doi: 10.1126/science.1117893
39. Bacac M, et al. CD20-TCB with obinutuzumab pretreatment as next-generation treatment of hematologic malignancies. Clin Cancer Res. 2018; doi: 10.1158/1078-0432.CCR-18-0455
40. Goubier A, et al. Fc-optimized anti-CD25 for tumour specific cell depletion. 2018
41. Roy G, et al. A novel bicistronic gene design couples stable cell line selection with a fucose switch in a designer CHO host to produce native and afucosylated glycoform antibodies. MAbs. 2018; doi: 10.1080/19420862.2018.1433975
42. Schlothauer T, et al. Novel human IgG1 and IgG4 Fc-engineered antibodies with completely abolished immune effector functions. Protein Eng Des Sel. 2016; doi: 10.1093/protein/gzw040
43. Kabsch, Wolfgang. XDS. Acta Crystallogr Sect D. 2010; D66:125–132.
44. McCoy AJ, et al. Phaser crystallographic software. J Appl Crystallogr. 2007; 40:658–674. [PubMed: 19461840]
45. Winn MD, et al. Overview of the CCP4 suite and current developments. Acta Crystallographica Section D: Biological Crystallography. 2011; :235–242. DOI: 10.1107/S0907444910045749 [PubMed: 21460441]
46. Bricogne, G, , et al. BUSTER version 2.9.5. Cambridge: United Kingdom Glob. Phasing Ltd; 2011.
47. Emsley P, Lohkamp B, Scott WG, Cowtan K. Features and development of Coot. Acta Crystallogr Sect D Biol Crystallogr. 2010; D66:486–501.
48. Parker, R; Fahl, S. P100 Exploring dissociated human tissues as an alternative to fresh tissue for multiple downstream applications. Poster Session presented at the Society for Immunotherapy of Cancer (SITC 2018) 33rd Annual Meeting; 2018.
49. Becht E, et al. Dimensionality reduction for visualizing single-cell data using UMAP. Nat Biotechnol. 2019; 37:38–44.
50. Van Gassen S, et al. FlowSOM: Using self-organizing maps for visualization and interpretation of cytometry data. Cytom Part A. 2015; 87:636–645.
51. Nowicka M, et al. CyTOF workflow: differential discovery in high-throughput high-dimensional cytometry datasets. F1000Research. 2017; 6:748. [PubMed: 28663787]
52. Lun ATL, Richard AC, Marioni JC. Testing for differential abundance in mass cytometry data. Nat Methods. 2017; 14:707–709. [PubMed: 28504682]

Europe PMC Funders Author Manuscripts

Europe PMC Funders Author Manuscripts

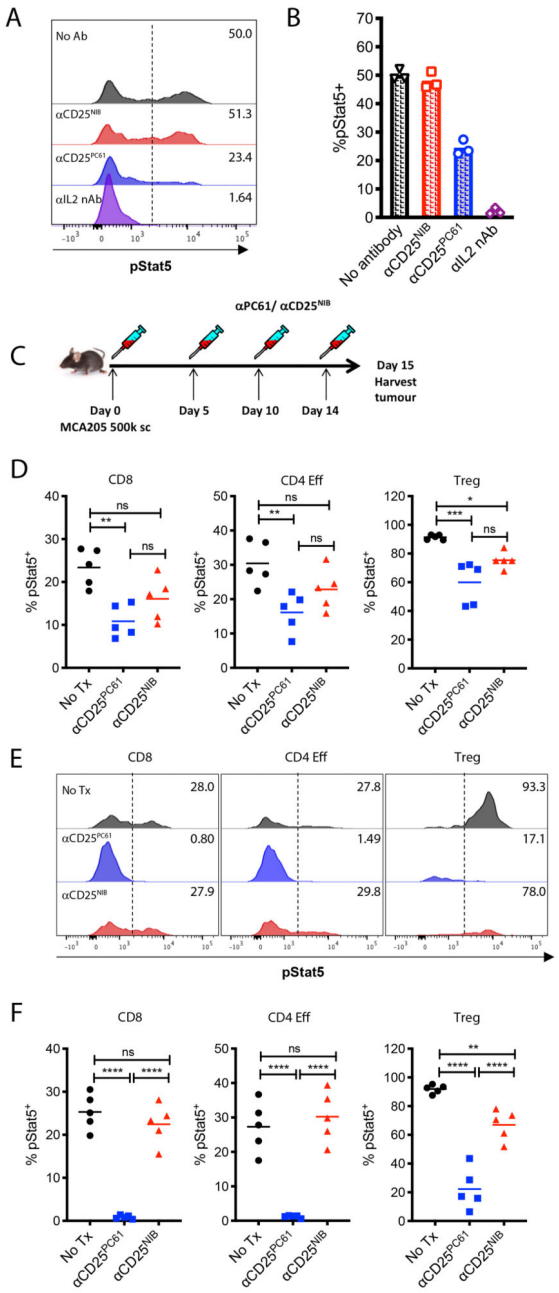

Fig. 1. Characterization of non-IL-2 blocking anti-mouse CD25 mAbs (αCD25^{NIB}).

(A) and (B) Pan T cells were isolated from splenocytes. 200,000 cells were plated and rested for 2 hours at 37°C. Antibodies were added at 50μg/ml and incubated with the cells for 30 mins at 37°C, following which cells were stimulated with IL-2 (50U/ml) for 10 mins at 37°C. Cells were stained for pStat5 as described and % Stat5 phosphorylation by different subsets of cells was recorded. **(A)** Representative histograms showing percentage of STAT5 phosphorylation observed in Tregs post-incubation with the antibodies listed. **(B)** Graph showing percentage of Stat5 phosphorylation observed in Tregs post-incubation with the

antibodies listed. Data represented as mean of triplicates ±SEM. p<0.0001. **(C) (D) (E) and (F)** C57BL6 mice were injected with 500,000 MCA205 tumor cells. Once tumors were palpable, mice were injected IP with αCD25^{PC61}or αCD25^{NIB} antibodies (200μg) on days 5, 10 and 14. Tumors were harvested on day 15 post-tumor inoculation **(C)**. Tumors were processed as described in materials and methods section. 200,000 cells were plated in a 96-well plate, antibody was either added at 50μg/ml for 30 mins **(E and F)** or omitted **(D)** followed by IL-2 stimulation (50U/ml) for 10 mins. Cells were fixed and stained for pSTAT5 as described. **(D)** Graphs showing percentage of STAT5 phosphorylation by CD8 (p=0.0021 between No Tx and αCD25^{PC61}), CD4 Eff (p=0.0077 between No Tx and αCD25^{PC61}) and Treg cells (p=0.0004 between No Tx and αCD25^{PC61} and p=0.0429 between No Tx and αCD25^{NIB}) (n=5 mice/group). **(E)** Representative histograms showing percentage of STAT5 phosphorylation by CD8, CD4 eff and Treg cells post-treatments with antibodies shown in **(F)**. **(F)** Graphs showing percentage of STAT5 phosphorylation by CD8, CD4 Eff and Treg cells (p=0.0080) between No Tx and αCD25^{NIB} (n=5 mice/group). All quantification plots: mean, 1-way ANOVA, Tukey's multiple comparisons test (ns=p>0.05, *p<0.05, **p<0.01, ***p<0.001, ****p<0.0001).

Europe PMC Funders Author Manuscripts

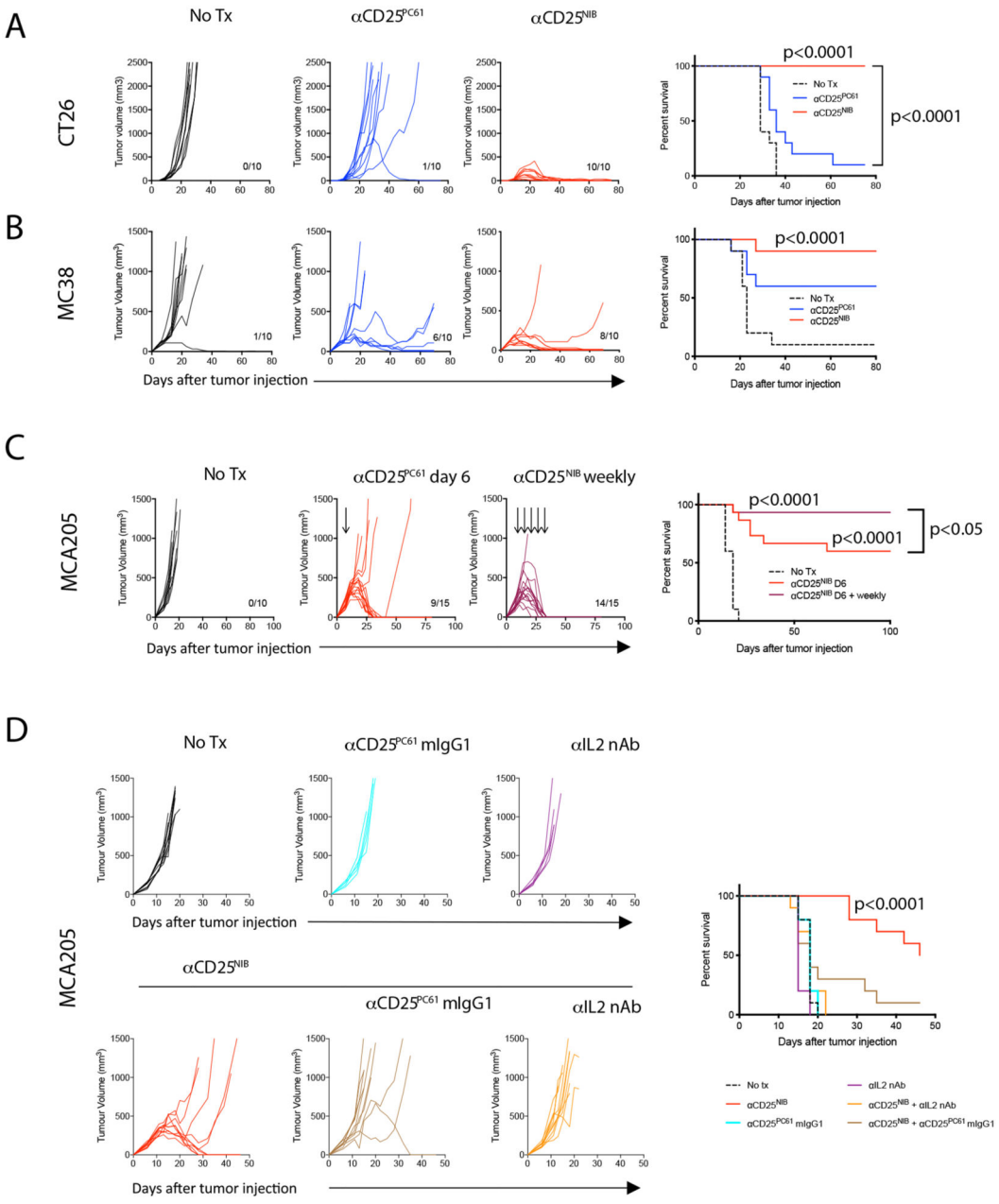

Fig. 2. Monotherapy αCD25^{NIB} drives rejection of established tumors in different mouse models.

(A) Balb/C mice were injected with 500,000 CT26 tumor cells. Treatment with αCD25^{PC61}/ αCD25^{NIB} was started on day 6 post-tumor inoculation. On the left, growth curves showing growth of tumor. On the right, survival. **(B)** C57BL6 mice were injected s.c. with 1,000,000 MC38 tumor cells in Matrigel. Treatment started on day 6 post-tumor inoculation. On the left, growth curves showing growth of tumor. On the right, survival**. (C)** C57BL6 mice were injected with 500,000 MCA205 tumor cells. Treatment started day 6, and continued weekly

afterwards for 4 consecutive weeks for the αCD25^{NIB} weekly group. On the right, survival, p=0.0399 between αCD25^{NIB} day 6 and αCD25^{NIB} weekly group. **(D)** C57BL6 mice were injected with 500,000 MCA205 tumor cells. Treatment started on day 6 post tumor inoculation. Survival of these mice shown on the right. Analysis of Kaplan-Meier survival curves was done using a two-sided log-rank test.

Europe PMC Funders Author Manuscripts

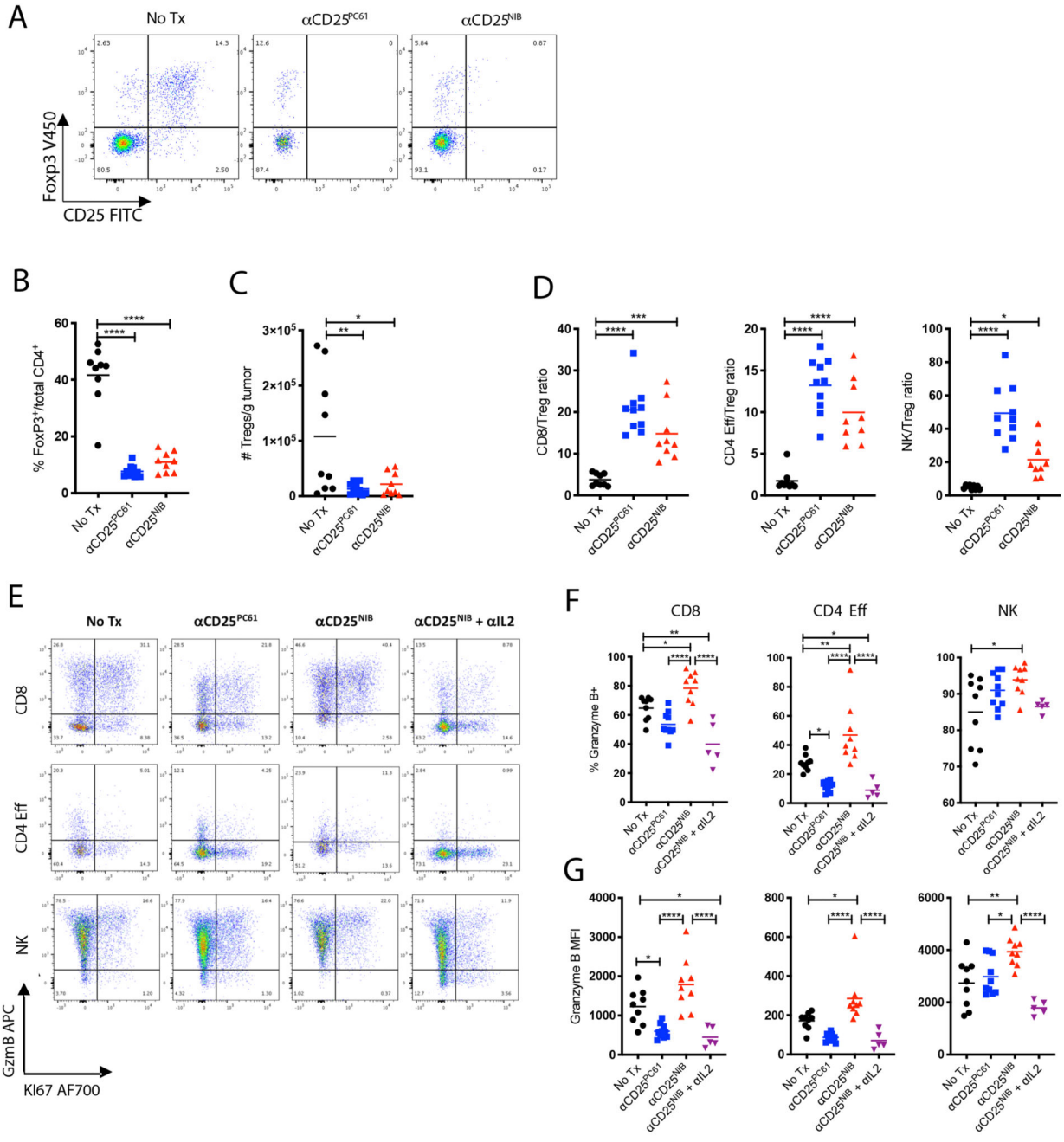

Fig. 3. αCD25^{NIB} and αCD25^{PC61} promote equivalent Treg depletion but different effector T cell activation in vivo.

C57BL6 mice were injected with 500,000 MCA205 tumor cells. Once tumors were palpable, on day 5, mice were injected IP with αCD25^{PC61}/αCD25^{NIB}/αCD25^{NIB} + αIL2 (200μg). Tumors and LN were harvested on day 12 post-tumor inoculation and processed as described in materials and methods. **(A)** Representative FACS plots showing expression of FoxP3 versus CD25 in CD4^{+} T cells. **(B)** Graph showing % FoxP3^{+} cells of total CD4^{+} cells. **(C)** Absolute number of Tregs shown as number of Tregs/g of tumor. P-value=0.0086

for No Tx vs αCD25^{PC61} and p=0.0204 for No Tx vs aCD25^{NIB} group.**(D)** Ratio of effector T cells over Tregs. On the left, p value for CD8/Treg ratio between No Tx and aCD25^{NIB}= 0.0003. On the right, p value for NK/Treg ratio between No Tx and αCD25^{NIB}=0.0170. **(E)** Representative FACS plots showing Granzyme B expression versus Ki67 expression in CD8, CD4 effectors and NK cells. **(F)** Graph showing percentage of Granzyme B^{+} cells in different effector subsets. In the CD8 subset, p-value between no Tx and αCD25NIB group=0.0452 and 0.0012 for No Tx vs αCD25^{NIB}+ αIL2 group. For the CD4 eff group, p value for No tx vs αCD25^{PC61}=0.0221, between No tx and αCD25^{NIB}=0.0059, between No tx and αCD25^{NIB} +αIL2=0.0276. For the NK subset, p value between the no tx and αCD25^{NIB} group=0.0232. **(G)** Graph showing the Mean Fluorescence Intensity of Granzyme B of the effector cells plotted in **(F)**. In the CD8 subset, p value for no tx vs αCD25^{PC61}=0.0222, and 0.0190 for No tx vs αCD25^{NIB} + αIL2 group. For the CD4 eff subset, p value between No tx and αCD25NIB=0.0112. For the NK subset, p-value for No tx vs αCD25^{NIB}=0.0057 and between αCD25^{PC61} vs αCD25^{NIB}=0.0295. All quantification plots: mean, 1-way ANOVA, Tukey's multiple comparison test (ns=p>0.05, *p<0.05, **p<0.01, ***p<0.001, ****p<0.0001).

Europe PMC Funders Author Manuscripts

Europe PMC Funders Author Manuscripts

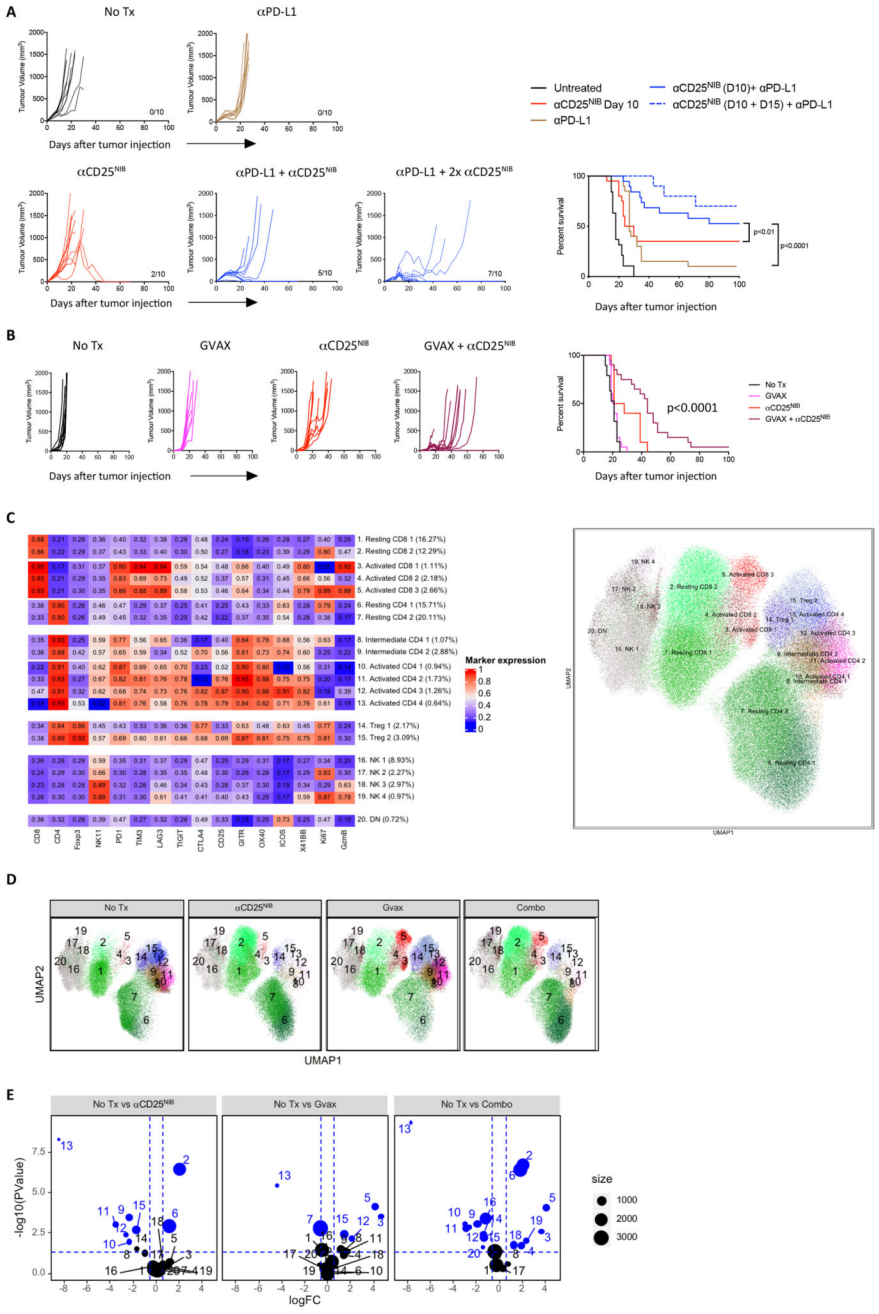

Fig. 4. αCD25^{NIB} as a substrate for combination immunotherapy

(A) C57BL6 mice were injected with 500,000 MCA205 tumor cells. Treatment with αPD-L1 (200μg) was started day 6, continued on days 9, 12 and 18. Groups receiving αCD25^{NIB} received either 1 dose at day 10 or an additional dose at day 15. Representative growth curves on the left, cumulative survival from 2 independent experiments of those mice is shown on the right. **(B)** C57BL6 mice were injected with 50,000 B16BL6 tumor cells. Treatment with Gvax was on days 6,9 and 12. αCD25^{NIB} (200μg) was administered on day 5. Cumulative survival of 2 independent experiments shown on the right, representative

growth curves on the left. Analysis of Kaplan-Meier survival curves was done using a two-sided log-rank test, p value between αCD25^{NIB} and αPD-L1+ αCD25^{NIB} group=0.0073. **(C) (D) and (E)** C57BL6 mice were injected with 50,000 B16BL6 tumor cells and treatment was administered as described in **(B)**. Tumors and LN were harvested on day 15 post-tumor inoculation and processed as described in materials and methods section. **(C)** Lymphoid cell populations integrated across all samples. Heatmap on the left shows min-max scaled, median marker expression of 20 subpopulations identified by unsupervised clustering. The identities of each cluster are annotated based on previously published analyses. The relationship between these clusters in UMAP dimension reduced space is shown in the plot on the right, and the effects of treatment on the lymphoid landscape are shown in **(D)**. Volcano plots in **(E)** represent differential cluster abundance in comparisons of each treatment group against control.

Europe PMC Funders Author Manuscripts

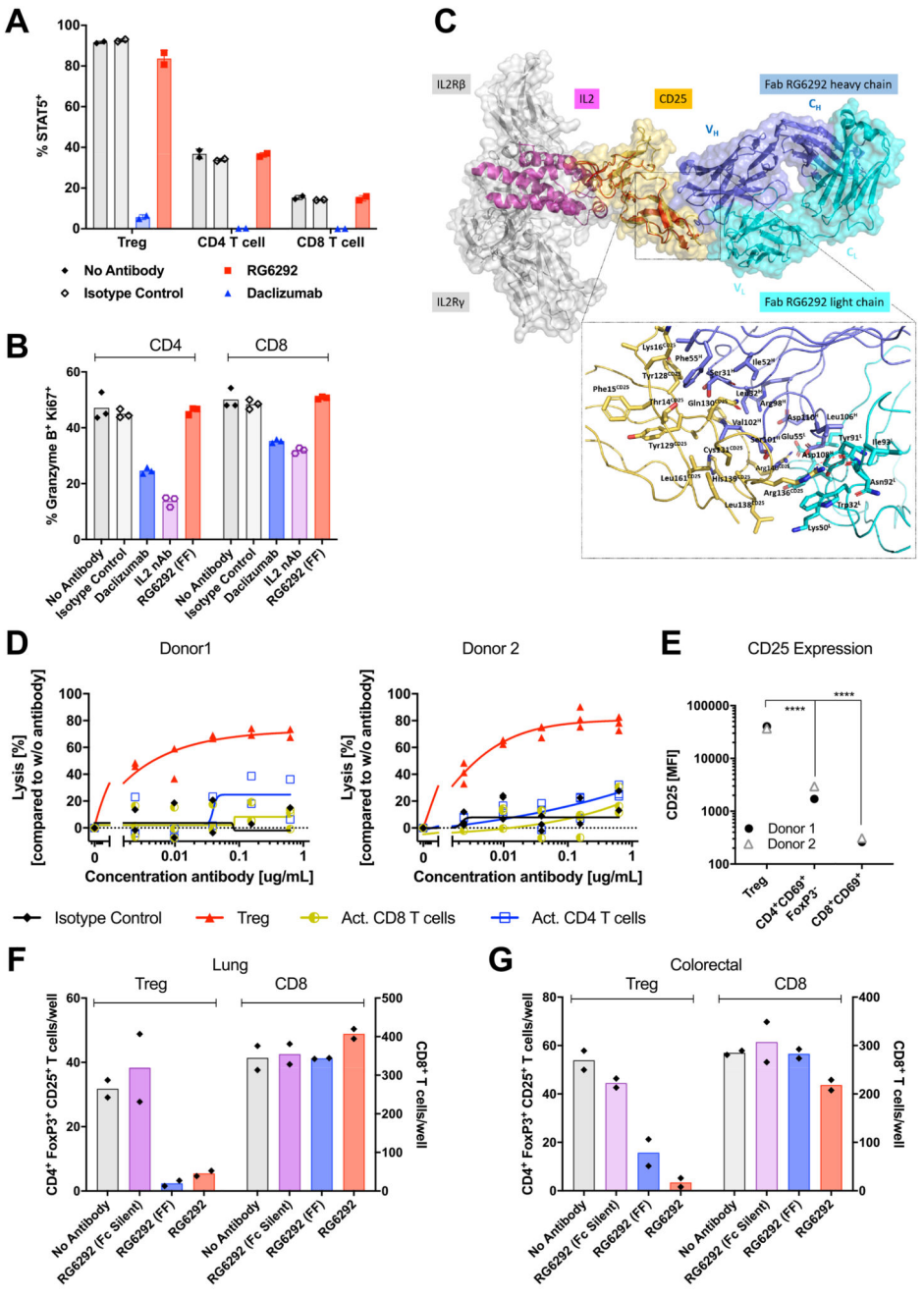

Fig. 5. A novel anti-human CD25^{NIB} promotes effective Treg depletion in patient-derived tumor samples in vitro.

(A) RG6292 did not block IL-2 signaling in a pSTAT5 assay using human PBMCs. Daclizumab was used as blocking control, human IgG1 isotype or untreated samples as reference control. Cells were incubated with 10 μg/ml antibody followed by 10 U/ml IL-2 for 10 min. pSTAT5 was analyzed on CD4$^+$, CD8$^+$ and Treg cells. Shown is the mean of technical duplicates with SD. **(B)** RG6292 did not negatively impact Granzyme B induction and proliferation of αCD3/αCD28 activated Pan T cells, other than addition of antibodies

Europe PMC Funders Author Manuscripts

either neutralizing IL-2 (αIL-2nAB) or blocking binding of IL2 to CD25 (Daclizumab). Antibodies were tested for 72 hours at 10 μg/ml. Shown is the mean of technical triplicates with SD. **(C)** The Fab fragment of RG6292 binds CD25 opposite of the IL2-CD25 interaction site. Shown is the superposition of the Fab RG6292 - CD25 structure with the IL2 quaternary signaling complex structure (PDB accession code 2B5I)[38]. The overlay was prepared using all atoms of CD25. IL2Rβ and IL2Rγ of the quaternary complex are shown as white transparent surface whereas IL2 is highlighted in magenta and CD25 in yellow/ red. The Fab light and heavy chains of RG6292 are colored in cyan and blue, respectively. The close-up section provides a detailed view onto the epitope and paratope area with residues labeled contributing to the interface. Further details are provided in the Supplementary Tables 2-5 and Extended Data Figure 5. **(D)** RG6292 mediated mostly depletion of CD25 high expressing regulatory T cells and not that of activated CD8 and CD4 effector T cells when present during polyclonal activation (αCD3 coated beads) of human PBMC. The counts of activated regulatory and non-regulatory $CD4^+$ and $CD8^+$ T cells within the PBMC sample were quantified on day 3 by flow cytometry and lysis by PBMC endogenous FcR+ cells was calculated. Shown is the mean of technical triplicates with SEM. **(E)** CD25 staining was performed to confirm target expression on Treg cells ($CD4^+$ $FoxP3^+$ CFSE high), activated CD4 ($CD4^+$ $FoxP3^-CD69^+$) and CD8 T cells ($CD8^+$ $CD69^+$) shown in **(D)**. **(F and G)** Graphs showing the killing of $FoxP3^+CD25^+$ cells within human tumors (frozen dissociated tumor cells obtained from Conversant Bio) supplemented with allogeneic NK cells mediated by RG6292 (and the fully fucosylated (FF) or Fc silent version of RG6292). Shown is the mean of technical duplicates with SD. All quantification plots: 2-way ANOVA, Sidak's multiple comparisons test (ns=p>0.05, *p<0.05, **p<0.01, ***p<0.001, ****p<0.0001).

Europe PMC Funders Author Manuscripts

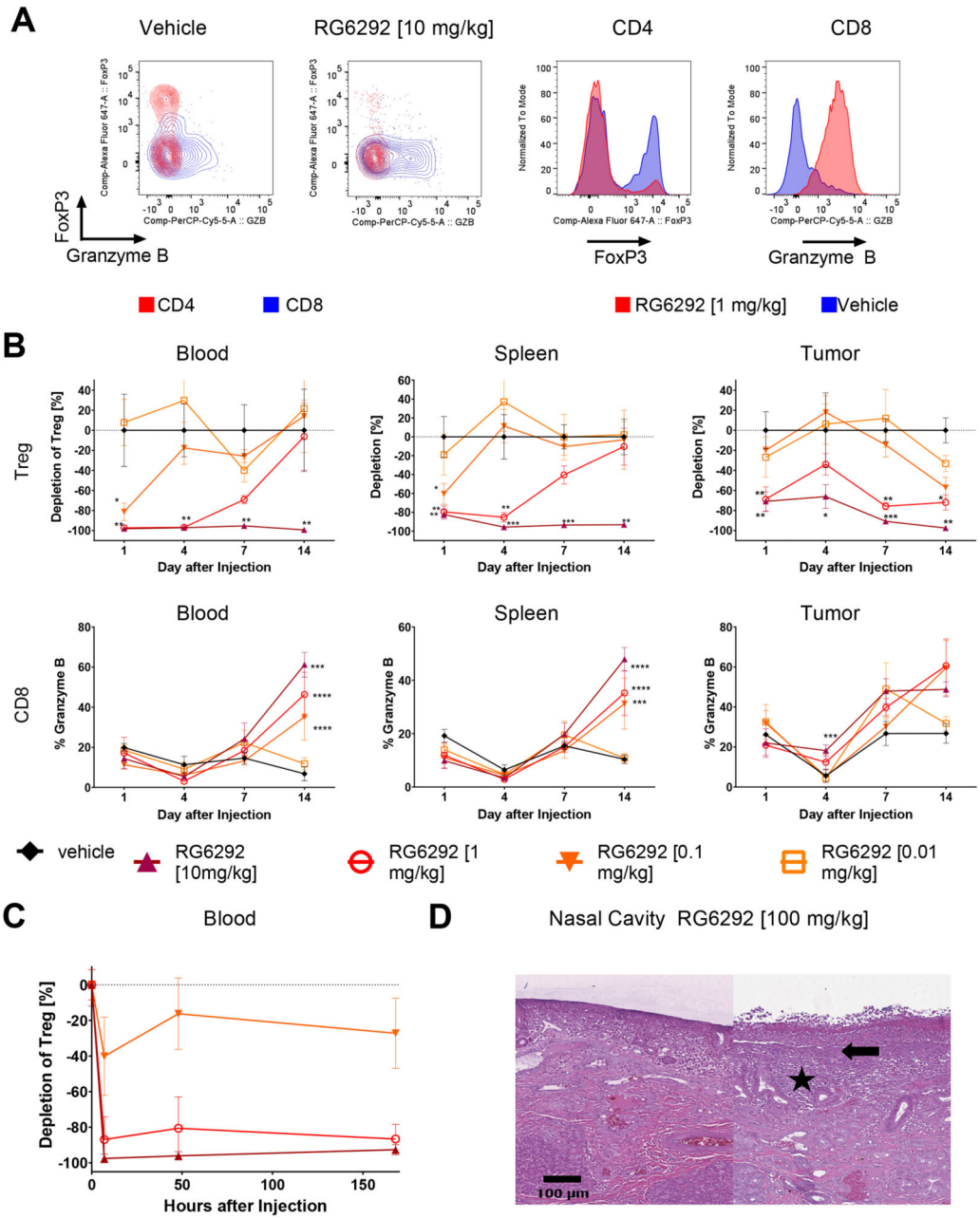

Fig. 6. Anti-human-CD25^{NIB} (RG6292) depletes Treg and drives T cell activation in tumor-bearing humanized mice and cynomolgus monkey.

(A and B) Stem cell humanized female NOG mice bearing an established s.c. BxPC-3 tumor were injected i.v. with vehicle, RG6292 [10, 1, 0.1 and 0.01 mg/kg]. Splenocytes, blood lymphocytes and tumor infiltrating lymphocytes were isolated 1, 4, 7 and 14 days after injection and evaluated for depletion of Tregs (huCD45$^+$, huCD3$^+$, huCD4$^+$, huCD25$^+$, huFoxP3$^+$) and activation of CD8$^+$ T cells (huCD45$^+$, huCD3$^+$, huCD8$^+$ GranzymeB$^+$). **(A)** Representative dot plots and histograms showing the decrease of FoxP3 and the increase of

Granzyme B expression on intra-tumoral $CD4^+$ and $CD8^+$ T cells 14 days after treatment with RG6292 compared to vehicle-injected animals. **(B)** Systemic and dose-dependent decrease in Tregs and an increase in activated $CD8^+$ T cells, respectively, was only evident after administration of RG6292. Each symbol represents the mean of 4 animals, and error bars indicate the SD. Statistical analysis (2 way ANOVA, Dunnet's multiple comparisons test (ns=p>0.05, *p<0.05, **p<0.01,) of RG6292 treated groups against the vehicle group is indicated. Actual p-values are summarized in tabular form in the supplementary data 1 **(C and D)** The toxicity and pharmacokinetic/pharmacodynamic (PK/PD) relationship of RG6292 was evaluated in cynomolgus monkeys following Q2W **(C)** or weekly **(D)** Repeated IV administrations during 4 **(D)** and 2 weeks **(C)**, respectively. Shown is the mean of three animals (male and female) +/- SD. **(D)** The only drug-related finding after application of supra-pharmacological doses (here 100 mg/kg/dose; Q2W) in the 4-week toxicity study, was an exacerbation of ulcerative/erosive rhinitis at 30 and 100 mg/kg shown in the right image (left image of nasal cavity from an unaffected animal for comparison), characterized by (partial) loss of epithelium (arrow) accompanied by inflammatory cell infiltrates (asterisk) in the nasal cavities of individual animals. Reversibility of the nasal lesions was demonstrated. The 4-week GLP toxicity study was conducted according to regulatory guidelines once.